J. Membrane Biol. 160, 59–76 (1997)

The Journal of
Membrane
Biology

High-Affinity NO_3^--H^+ Cotransport in the Fungus *Neurospora:* Induction and Control by pH and Membrane Voltage

M.R. Blatt, L. Maurousset*, A.A. Meharg**
Laboratory of Plant Physiology and Biophysics, Wye College, University of London, Wye, Kent TN25 5AH, UK

Received: 17 March 1997/Revised: 20 June 1997

Abstract. High-affinity nitrate transport was examined in intact hyphae of *Neurospora crassa* using electrophysiological recordings to characterize the response of the plasma membrane to NO_3^- challenge and to quantify transport activity. The NO_3^--associated membrane current was determined using a three electrode voltage clamp to bring membrane voltage under experimental control and to compensate for current dissipation along the longitudinal cell axis. Nitrate transport was evident in hyphae transferred to NO_3^--free, N-limited medium for 15 hr, and in hyphae grown in the absence of a nitrogen source after a single 2-min exposure to 100 μM NO_3^-. In the latter, induction showed a latency of 40–80 min and rose in scalar fashion with full transport activity measurable approx. 100 min after first exposure to NO_3^-; it was marked by the appearance of a pronounced sensitivity of membrane voltage to extracellular NO_3^- additions which, after induction, resulted in reversible membrane depolarizations of (+)54–85 mV in the presence of 50 μM NO_3^-; and it was suppressed when NH_4^+ was present during the first, inductive exposure to NO_3^-. Voltage clamp measurements carried out immediately before and following NO_3^- additions showed that the NO_3^--evoked depolarizations were the consequence of an inward-directed current that appeared in parallel with the depolarizations across the entire range of accessible voltages (−400 to +100 mV). Measurements of NO_3^- uptake using NO_3^--selective macroelectrodes indicated a charge stoichiometry for NO_3^- transport of 1(+):1(NO_3^-) with common K_m and J_{max} values around 25 μM and 75 pmol NO_3^- $cm^{-2}sec^{-1}$, respectively, and combined measurements of pH_o and $[NO_3^-]_o$ showed a net uptake of approx. 1 H^+ with each NO_3^- anion. Analysis of the NO_3^- current demonstrated a pronounced voltage sensitivity within the normal physiological range between −300 and −100 mV as well as interactions between the kinetic parameters of membrane voltage, pH_o and $[NO_3^-]_o$. Increasing the bathing pH from 5.5 to 8.0 reduced the current and the associated membrane depolarizations 2- to 4-fold. At a constant pH_o of 6.1, driving the membrane voltage from −350 to −150 mV resulted in an approx. 3-fold reduction in the maximum current and a 5-fold rise in the apparent affinity for NO_3^-. By contrast, the same depolarization effected an approx. 20% fall in the K_m for transport as a function in $[H^+]_o$. These, and additional results are consistent with a charge-coupling stoichiometry of 2(H^+) per NO_3^- anion transported across the membrane, and implicate a carrier cycle in which NO_3^- binding is kinetically adjacent to the rate-limiting step of membrane charge transit. The data concur with previous studies demonstrating a pronounced voltage-dependence to high-affinity NO_3^- transport system in *Arabidopsis*, and underline the importance of voltage as a kinetic factor controlling NO_3^- transport; finally, they distinguish metabolite repression of NO_3^- transport induction from its sensitivity to metabolic blockade and competition with the uptake of other substrates that draw on membrane voltage as a kinetic substrate.

Key words: Plasma membrane NO_3^--H^+ cotransport — *Neurospora crassa* — NH_4^+ repression — Metabolic blockade — Voltage clamp — Reaction kinetic model

Introduction

Nitrate uptake, its reduction to nitrite and subsequently to ammonium play an important role in maintaining the

* *Present address:* UA CNRS 574, Laboratoire de Biologie et Physiologie Vegetales, Universite de Poitiers, 86000 Poitiers, France

** *Present address:* Institute of Terrestrial Ecology, Monds'Wood, Abbots Ripton, Huntingdon, Cambs. PE17 2LS UK

Correspondence to: M.R. Blatt

nitrogen status of plants, algae and fungi (Ullrich, 1987). In every case, high-affinity transport of NO_3^- is manifest under *N*-limiting conditions and shares similar characteristics: the capacity for NO_3^- scavenging is generally evident — or is greatly enhanced — following NO_3^- exposures (Schloemer & Garrett, 1974; Doddema, Hofstra & Feenstra, 1978; Tischner et al., 1993; MacKown, 1987; Glass et al., 1990; Meharg & Blatt, 1995). Induction of NO_3^- transport is sensitive to inhibitors of protein synthesis (Heimer & Filner, 1970; Schloemer & Garrett, 1974) and is marked by often complex metabolite repression (Goldsmith et al., 1973; Doddema et al., 1978; Clarkson, Saker & Purves, 1989; Rufty, Jr. Mackown & Israel, 1990; Tischner et al., 1993; Henriksen & Spanswick, 1993). Finally, once induced, transport exhibits an apparent affinity for NO_3^- typically in the range of 20–50 μM (Heimer & Filner, 1970; Schloemer & Garrett, 1974; Rao & Rains, 1976; Goyal & Huffaker, 1986; Ullrich, 1987; MacKown, 1987; Meharg & Blatt, 1995).

Early studies established a requirement for energy input, demonstrating that NO_3^- uptake is sensitive to metabolic poisons and uncouplers, and subsequent work has supported, albeit indirectly, a coupling of NO_3^- transport with H^+ movement across the plasma membrane (Heimer & Filner, 1970; Schloemer & Garrett, 1974; Rao & Rains, 1976; Doddema & Telkamp, 1979; McClure et al., 1990; Ullrich & Novacky, 1990; Glass et al., 1990).

Strong support for coupling to the movement of two H^+ has come from recent voltage-clamp analyses of NO_3^- transport across root hairs of *Arabidopsis* (Meharg & Blatt, 1995). However, these data have also highlighted features of high-affinity NO_3^- transport that distinguish it from the majority of H^+-coupled transporters previously identified either in plants or fungi. Proton-coupled transport of amino acids (Schwab & Komor, 1978; Felle, 1981; Sanders, Slogman & Paul, 1983), sugars (Schwab & Komor, 1978), and of the inorganic anion Cl^- (Sanders & Hansen, 1981; Beilby & Walker, 1981) in large measure have shown only limited sensitivity to membrane voltage. By contrast, in the root hairs NO_3^- transport displayed a pronounced voltage dependence within the physiological voltage range. Furthermore, kinetic analysis indicated a simple, first-order dependence on H^+ binding for transport despite coupling with two H^+ (Meharg & Blatt, 1995), pointing to a kinetic isolation of rate-limiting cation (H^+)-binding analogous to ion-coupled K^+ transporters in *Neurospora* and *Chara* which also entail two cation-binding steps (Blatt et al., 1987; McCulloch, Beilby & Walker, 1990).

These results have demonstrated that membrane voltage can limit NO_3^- transport and explain why NO_3^- uptake should be restricted at neutral to alkaline pH, even in the face of a large electrical driving force (Ullrich & Novacky, 1981; Ullrich & Novacky, 1990; Meharg & Blatt, 1995). Nonetheless, they leave as many issues unaddressed, notably the relationship between the voltage-dependence of NO_3^- uptake, its probable kinetic suppression by metabolites which may themselves influence membrane voltage (Ullrich et al., 1984; Deane-Drummond, 1985; Henriksen, Bloom & Spanswick, 1990), and the depression of NO_3^- transport induction by the same metabolites (Goldsmith et al., 1973; Doddema et al., 1978; Clarkson et al., 1989; Rufty, Jr. et al., 1990; Tischner et al., 1993; Henriksen & Spanswick, 1993). Indeed, external NH_4^+ as well as a range of amino acids, notably glutamine and asparagine, are known to influence the induction of NO_3^- transport (Ullrich et al., 1984*b;* Lee & Drew, 1989*b;* Heimer & Filner, 1970*b;* Goldsmith et al., 1973*b;* Privalle et al., 1989; Schloemer & Garrett, 1974*b*). Yet these compounds, especially NH_4^+, may also affect NO_3^- uptake once the transporter is induced, simply by virtue of the fact that they draw on a common ''substrate'' for transport, namely the membrane potential.

To address these questions, we have examined the characteristics of NO_3^- transport in the fungus *Neurospora,* for which a large body of quantitative information on ATP- and ion-coupled transport is already to hand. This paper explores the energetic requirements for NO_3^- transport, its voltage- and H^+-dependent kinetic characteristics following induction by N-starvation. Additionally, we outline experiments directed to characterizing NO_3^- transport induction in *Neurospora*, and especially to the effects of one metabolite, NH_4^+, on its expression distinct from any action on membrane voltage. The results demonstrate, among others, that the effect of NH_4^+ on transporter induction is separable from its impact on membrane voltage and NO_3^- transport in fully-induced hyphae.

Materials and Methods

Cell Growth and Handling

The wild-type strain 74A of *Neurospora crassa* obtained from Professor Fincham (Genetics, Cambridge) was used throughout these experiments. Cultures were maintained on slants of Vogel's medium with 2% glucose and with NH_4^+ as the sole nitrogen source [AmVM (Rodriguez-Navarro et al., 1986); *see* Table]. Cells for (chemical) flux measurements were grown from the N-starved tissue to give a mycelial suspension of cells (Slayman & Tatum, 1968; Slayman & Slayman, 1974).

To obtain satisfactory growth, both of these preparations and mycelia for electrical recordings were subcultured on media containing NH_4^+ and transferred to nominally N-free media (-NVM or NitVM to induce the transport system; *see* Table) 15 hr prior to the start of experiments. Mycelial suspension cultures were prepared by innoculating 25 ml AmVM medium at 1×10^6 conidia/ml in flasks that were then maintained on a rotary shaker (120 cycles/min) at 26°C. The cultures were removed after 24 hr, filtered onto 5 μm HA Millipore

Table. Composition of growth media[a] and experimental buffers (values in mM)

	AmVM	-NVM	NitVM	K^+/Ca^{2+}-MES
Na^+	0[b]	0	0.1	0
K^+	0.3	0.3	0.3	2
NH_4^+	40	0	0	0
Ca^{2+}	0.1	0.1	0.1	1.3
Mg^{2+}	0.8	0.8	0.8	0
Cl^-	0.5	0	0	0
NO_3^-	0	0	0.1	0
SO_4^{2-}	0.8	0.8	0.8	0
Phosphate	15	15	15	0
Citrate	8.4	8.4	8.4	0
MES	0	0	0	5
Sucrose (%)	2	2	2	0 or 2
pH	5.8	5.8	5.8	6.1

[a] Modified from the ''N'' minimal medium of Vogel (1956) and containing the same trace elements and biotin.

[b] Designation means no added salt, except for NO_3^- in which case concentrations were always below measurable levels (*see* Materials and Methods).

filters (Millipore, Poole), and washed thoroughly with -NVM medium before being resuspensed in NitVM.

Shaking cultures were harvested by filtration as before, washed with K^+Ca^{2+}-MES buffer (Table) — comprising 5 mM 2[N-morpholino]ethane sulphonic acid (MES) titrated to pH 6.1 using $Ca(OH)_2$ ($[Ca^{2+}] \sim 1$ mM) with 0.2 mM K^+ added as K^+-MES titrated to pH 6.1 — and resuspended in the same buffer plus 1% glucose. Growth was reduced on limiting nitrogen, and little further increase in cell weight or volume was observed (*data not shown*). After 15 hr, residual NO_3^- was ≈10 μM in cultures transferred to NitVM and was essentially undetectable in cultures transferred to −NVM using either microelectrode (below) or photochemical assays (Goldsmith et al., 1973). At final harvest, cells in shaking cultures were largely unbranched filaments, 3–5 μm in diameter and 80–200 μm in length.

Electrical recordings were carried out using hyphae grown on 1% Bactoagar (Difco Laboratories, Detroit, MI). For this purpose, subcultures were made from agar plugs innoculated on AmVM agar plates and were grown at 26°C for 24 hr before a second agar plug was innoculated on a −NVM agar plate. After a further 24-hr growth, blocks of agar containing the leading edge of hyphal growth were removed and mounted for electrical recording.

The preferred experimental buffer was K^+Ca^{2+}-MES, as Cl^- has been suggested to interfere with NO_3^- uptake (Deane-Drummond & Glass, 1982) and several anions are known to interfere with the sensor (methyltridodecylammonium nitrate) of NO_3^- selective electrodes (Ullrich, 1987; Wegmann et al., 1984). In some experiments the MES buffer was replaced with ACES (N-[2acetamide]-2-aminoethane sulfonic acid; pK_a 6.8), HEPES (N-[2-hydroxyethyl]piperazine-N′-[2-ethane] sulfonic acid; pK_a 7.4), and EPPES (N-[2-hydroxyethyl]-piperazine-N′-[3-propane] sulfonic acid; pK_a 8.0) titrated to the pK_as with KOH and $Ca(OH)_2$ to give $[K^+] = 2$ mM and $[Ca^{2+}] \sim 1$ mM. Electrical measurements at pH 5.5 were obtained in K^+Ca^{2+}-MES buffer, but with the MES concentration raised to give the same cation concentrations. Ammonium was added during experiments as NH_4^+-MES from a 20 mM stock solution (20 mM MES buffer, titrated to pH 6.1 with NH_4OH; final $[NH_4^+] = 10$ mM). All chemicals were analytical grade or better, and were obtained from Fluka (Glossop, Derbyshire, UK), Sigma Chemical (St. Louis, MO) or from BDH Ltd. (Poole, Dorset, UK).

Flux Experiments

After harvesting, all cultures were resuspended in K^+/Ca^{2+}-MES buffer (densities of 0.1–1.0 mg dry weight/ml) and preincubated for 20–30 min with gentle agitation by aeration in a water-bath at 25°C. Free NO_3^- concentration in the bath was monitored continuously using a Corning NO_3^--selective membrane electrode (against a 100 mM $NaNO_3$/100 mM KCl electrolyte) and Delta 250 pION meter (Corning, NY) connected to a strip chart recorder. An Ag|AgCl|1M KCl halfcell served as the reference, and connection to the bath was made with a 2% agar bridge containing 50 mM K_2SO_4. Nitrate was added as the Na^+ salt, and NO_3^- uptake monitored as its disappearance from the bath. Electrode calibrations were carried out in the flux buffer as described by Wegmann et al. (1984), both in the absence and presence of 50 mM K_2SO_4. The NO_3^--selective electrodes routinely gave slopes of (−)53–55 mV/$[NO_3^-]$ decade at NO_3^- concentrations of 10^{-5} M and above. Between 10^{-5} and 10^{-6} M NO_3^- the signal generally decayed to (−)15–20 mV/$[NO_3^-]$ decade both in the presence and absence of K_2SO_4 additions.

For comparison with intracellular recordings only initial rates of uptake were used when $[NO_3^-]_o$ was within 90% of the maximum following each addition and flux was normalized to the cell surface area. Following experiments, suspension culture cells were filtered, rinsed with distilled water, dried overnight at 95°C and weighed. Cytoplasmic volumes were calculated from the ratio of intracellular water/dry weight (= 2.54), and corresponding surface areas were determined from the average cylindrical cell diameter of 4 μm, given a surface/volume ratio of 1×10^4 cm^2/cm^3 (Slayman & Tatum, 1968; Slayman & Slayman, 1974; Rodriguez-Navarro et al., 1986).

In some experiments H^+ release was followed simultaneously with measurement of net uptake of NO_3^- using a commercial pH-electrode (Corning pH-Microcombination) and second strip-chart recorder. In these experiments, the reference solution of the pH electrode was replaced with 100 mM K_2SO_4 at the glass frit to avoid Cl^- interference and 100 mM KCl layered above to maintain reversibility. A K^+Ca^{2+}-MES buffer was used, but at a buffer concentration of 0.5 mM with the additions of 1 mM K_2SO_4 and $CaSO_4$. This low-pH buffer served both to minimize errors from CO_2 absorption and to increase the sensitivity of the H^+ measurements by reducing the buffer capacity.

Microelectrodes

Intracellular recordings were obtained using a combination of single- and double-barrelled microelectrodes (Blatt, 1991, 1992; Meharg, Maurousset & Blatt, 1994). Microelectrodes (barrels) were filled with 200 mM K^+-acetate, pH 7.2., to minimize salt leakage and salt-loading artifacts associated with the Cl^- anion (Blatt & Slayman, 1983; Blatt, 1987*a*) without imposing a significant acid or alkaline load (Blatt & Armstrong, 1993). Connection to the amplifier headstage was via a 1 M KCl|Ag-AgCl halfcell, and a matching halfcell and 1 M KCl-agar bridge served as the reference (bath) electrode.

Electrical

All experiments were carried out in fast-flowing buffer solutions (approx. 10 chamber volumes/min). Mechanical, electrical and software design have been described in detail (Blatt, 1987, 1990, 1991), with the addition that a second, single-barrelled microelectrode was placed in the adjacent cell of the same hypha. Thus, recordings routinely en-

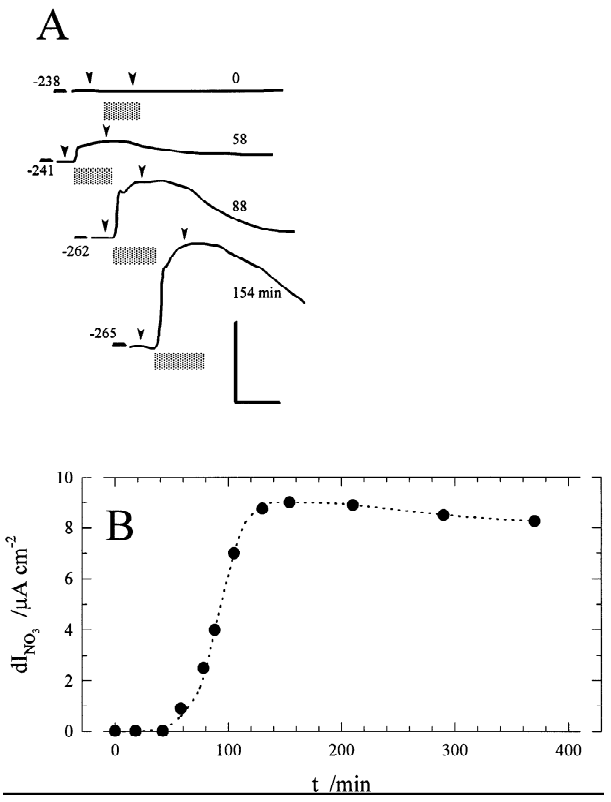

Fig. 1. NO_3^- transport activity is expressed following a brief exposure to NO_3^-. Data from one *Neurospora* hypha in 10 mM K^+/Ca^{2+}-MES, pH 6.1, challenged periodically with 100 μM NO_3^-. (*A*) Membrane voltage traces recorded during NO_3^- exposures at times indicated on right. Voltages in mV on left. Additions of 100 μM NO_3^- indicated by stippled bars below each trace. Carats mark times of voltage clamp scans (masked from traces). Scale: vertical, 50 mV; horizontal, 3 min. (*B*) Time course for NO_3^- transport induction determined as the current difference, δI_{NO3}, determined at −250 mV under voltage clamp ± NO_3^- (*see also* Fig. 3).

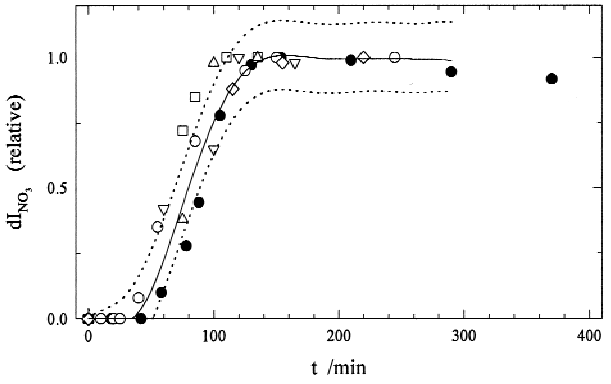

Fig. 2. Induction of NO_3^- transport in *Neurospora* follows a single exposure to NO_3^-. Time course for induction taken from δI_{NO3} at −250 mV following 2-min inductive pulses of 100 μM NO_3^- at t = 0 min and normalized to measurements at time points at 100–150 min thereafter. Data points shown are from 6 hyphae in 10 mM K^+/Ca^{2+}-MES pH 6.1, including data from Fig. 1 (●). Curves are best, 5th-order polynomial fittings for induction time course taken from the membrane voltage response to NO_3^- in all experiments (solid curve) and the corresponding 95% prediction interval (dotted curves). Note the roughly equivalent induction time courses also when hyphae were subsequently challenged with NO_3^- only after 78 min (□) and 118 min (◇).

tailed two impalements, the double-barrelled microelectrode being used to pass current and record voltage. Membrane potentials measured both by the simple microelectrode and by the voltage-recording barrel of the double-barrelled microelectrode were logged on a Kipp/Zonen BD1200 two-pen strip-chart recorder (Kipp/Zonen, Malsfeld, FRG).

Current-voltage (*I–V*) relations were determined under voltage clamp by a three-electrode method (Meharg & Blatt, 1995) with the voltage clamp under microprocessor control using a WyeScience μP amplifier and μLAB analog/digital interface and software (WyeScience, Wye, Kent, UK). The clamp comparator utilized the voltage recorded near the point of current injection, and voltage deflections in the adjacent cell were used to correct for axial current dissipation (Gradmann et al., 1978). Steady-state *I–V* relations were recorded by clamping cells to a bipolar staircase of command voltages (Meharg & Blatt, 1995; Blatt, 1987; Blatt et al., 1987). Steps alternated positive and negative from the free-running membrane potential, V_m (typically 20 bipolar pulse-pairs of 200 msec duration) and were separated by equivalent periods when the membrane was clamped to V_m. The current signal was filtered by a 6-pole Butterworth filter at 1 kHz (-3dB) before sampling, and currents and voltages were recorded during the final 10-msec of each pulse.

Numerical Analysis

Data analysis was carried out by nonlinear, least-squares (Marquardt, 1963) and, where appropriate, results are reported as the mean ± SE of (*n*) observations.

Results

General Electrical Characteristics of NO_3^- Transport in N-starved Cells

Expression of NO_3^- transport activity in *Neurospora*, grown on NH_4^+ as a nitrogen source and N-starved over 15 hr, was found to require prior exposure to the anion and full activity was attained within a three-hour period thereafter [*see also* (Schloemer & Garrett, 1974)]. Figure 1 details the response of one hypha to NO_3^- over a period of more than 6 hr (*see also* Fig. 2). Following impalement, adding 100 μM NO_3^- (2.8 min) had no effect on membrane voltage (Fig. 1*A*) or on total membrane current under voltage clamp (*not shown*). A similar lack of effect was observed during two additional challenges (<2 min each) over the next 40 min. After 58 min a fourth exposure to 100 μM NO_3^- resulted in a 6 mV depolarization and, when the membrane was clamped to −250 mV near the free-running voltage, yielded a small, and inward-directed current (Fig. 1*B*). Subsequent exposures to NO_3^- showed both membrane depolarizations and the associated current increased to maxima after approximately 2 hr, remaining roughly constant thereafter

(Fig. 1*B*). Similar results were obtained in separate experiments with 20 hyphae (*not shown*). Induction of the NO_3^- current was achieved with initial exposures to 100 μM NO_3^- as short as 2 min; it could be suppressed with concurrent, but not subsequent exposures to NH_4^+ (*see* Fig. 7); and neither the lag time nor the rate at which the transport activity appeared were sensitive to subsequent NO_3^- challenge (Fig. 2).

Once induced, challenge of *Neurospora* with as little as 6 μM NO_3^- resulted in rapid membrane depolarizations, and the steady-state change in V_m increased with the concentration of NO_3^- present in the bath. On washing the NO_3^- from the bath, V_m recovered its initial value, although complete repolarization generally required 5–8 min when exposures were prolonged for more than 2–3 min (*cf.* Figs. 1 and 3). Such delays in recovery were found to be independent of superfusion rate (*data not shown*). These characteristics suggested a compound response to NO_3^- following the longer exposures, much as previously inferred from observations of NO_3^--evoked voltage changes in maize, *Limnobium* and *Lemna* (Ullrich & Novacky, 1981; Ullrich & Novacky, 1990; McClure et al., 1990). Challenges with NO_3^- in subsequent experiments were therefore limited to periods of 3 min or less whenever possible.

Voltage Dependence of the NO_3^--Evoked Current

Voltage recordings such as those shown in Fig. 1 indicated that adding NO_3^- engendered a significant current to depolarize V_m. Because a significant body of evidence — albeit, largely indirect [but *see* (Eddy & Hopkins, 1985)] — already pointed to ion-driven mechanisms for NO_3^- transport in other fungi, algae and higher-plants (*see* Introduction) and to an energy-dependence for NO_3^- uptake in *Neurospora* (Schloemer & Garrett, 1974), we chose to examine the characteristics of the NO_3^--evoked current directly, making use of a three-electrode voltage clamp (Meharg & Blatt, 1995; Gradmann et al., 1978). Measurements carried out in this way would yield a description of the NO_3^--evoked current at each clamp voltage, so obviating difficulties in quantification entailed by changes of free-running membrane potential on adding NO_3^-, and would allow direct comparison with NO_3^- (chemical) flux measurements in determining the apparent charge stoichiometry for NO_3^- transport.

For this purpose, steady-state current across the hyphal plasma membrane was recorded at intervals throughout these experiments before, during and after exposures to NO_3^-. In each case, the membrane was driven in discrete steps over the widest possible voltage range, nominally to voltages between −400 and +100 mV. In order to estimate the NO_3^--induced currents, independent of other transport activity at the *Neurospora* membrane, difference currents (δ*I*) were calculated at each clamp voltage by subtracting the control current recorded before NO_3^- addition from the corresponding currents determined in the presence of the anion. Two assumptions underlie the approach in this case: (i) the effect of NO_3^- addition should be limited primarily to the specific transport process of interest, and (ii) in the absence of NO_3^- outside, current associated with forward operation of the transporter should be zero. These conditions were met for short-term exposures to NO_3^-. In its absence, the principle components of the current-voltage (*I–V*) relationships were accounted for by the characteristics of the *Neurospora* H^+-ATPase and a nonlinear leak conductance (Blatt et al., 1990; Slayman, Bertl & Blatt, 1994; Blatt & Slayman, 1987). Also, following brief exposures (<3 min) to NO_3^- the membrane *I–V* characteristics normally recovered to the control state on NO_3^- washout (*not shown*). Thus, the initial depolarization in NO_3^- was reasonably accounted for as a direct result of substrate addition and its consequence in engaging the kinetics for NO_3^- transport.

Figure 3 shows the effects of adding 12–100 μM NO_3^- on total membrane current (Fig. 3*A*) recorded from one *Neurospora* hypha, and the difference current-voltage (δ*I–V*) characteristics derived from each after subtracting the control currents recorded in the absence of NO_3^- (Fig. 3B). The inset (Fig. 3*A*, *above*) shows the free-running membrane voltage trace recorded before, during and after exposure to 100 μM NO_3^-. At this, and the other NO_3^- concentrations membrane depolarization was associated with a downward (negative-going) shift in the membrane *I–V* curve (Fig. 3*A*). NO_3^- additions led to an increase in membrane conductance, notably at voltages negative of −150 mV, but had little effect or even reduced the overall membrane conductance at voltages positive-going from this value, indicating a voltage-dependence to the NO_3^- current (Fig. 3*B*). Thus, for 100 μM NO_3^-, subtraction yielded a NO_3^- difference current, δI_{NO_3}, of (−)10.6 μA cm^{-2} at −350 mV which was reduced to (−)3.2 μA cm^{-2} at −150 mV. Qualitatively comparable responses were observed at each NO_3^- concentration, with lower concentrations resulting in correspondingly smaller changes in the total membrane *I–V* characteristic (Fig. 3*A*) and NO_3^- difference currents (Fig. 3*B*). Similar results were obtained in all 34 cells subjected to voltage clamp analysis under these conditions, and when the order of additions was reversed. A mean δI_{NO_3} of 8.3 ± 0.8 μA cm^{-2} was obtained at a clamp voltage of −200 mV when bathed in 5 mM Ca^{2+}-MES/0.2 mM K^+-MES, pH 6.1, with 100 μM NO_3^-.

It was notable that NO_3^- additions in every case gave δ*I–V* curves showing an *increase* in the magnitude of inward-directed current, even at the most positive-going clamp voltages (*cf.* Fig. 3*B*). On a basis of thermodynamic considerations alone, currents associated with

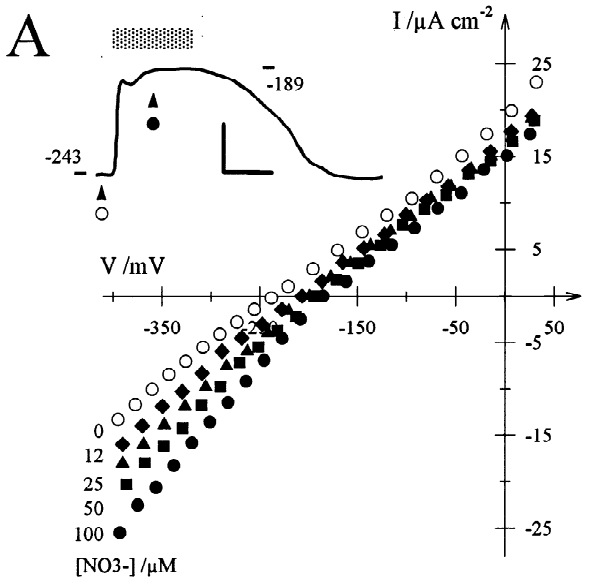

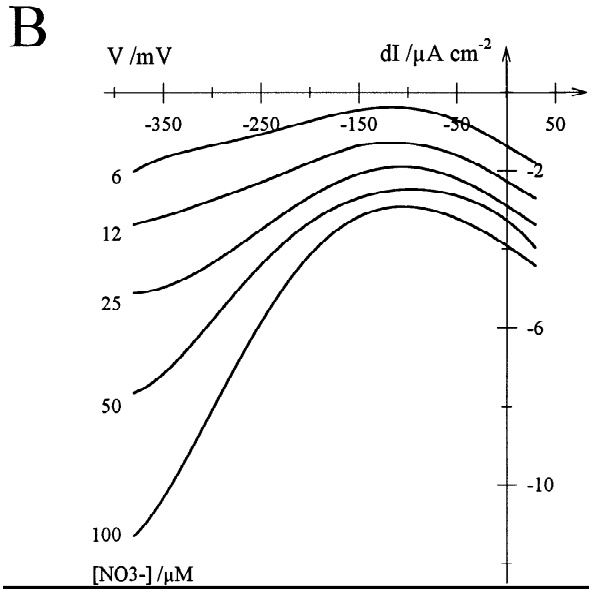

Fig. 3. NO_3^--evoked current in *Neurospora* shows appreciable voltage sensitivity within the normal physiological voltage range. Steady-state current-voltage (*I–V*) and difference-current-voltage (δ*I–V*) curves as a function of NO_3^- concentration in the bath. Data from one *Neurospora* hypha (*A*) *I–V* curves determined at time points before (○) and during challenge with 12 μM (♦), 25 μM (▲), 50 μM (■) and 100 μM (●) NO_3^- against a background of K^+/Ca^{2+}-MES buffer, pH 6.1 NO_3^- concentrations indicated on left. *Inset:* Membrane voltage response to 100 μM NO_3^- addition. Voltages indicated in mV. Times of *I–V* scans indicated by carats and cross-referenced by symbol to the *I–V* curves. Scale: 25 mV and 2 min. (*B*) δ*I–V* curves derived by subtracting currents recorded before, from those recorded during NO_3^- exposures in *A* and including additional data for 6 μM NO_3^-. NO_3^- concentrations indicated on left. Note the different current scale.

NO_3^- transport at these external NO_3^- concentrations might be expected to *cross* the voltage axis at equilibrium potentials near 0 to +50 mV, assuming an internal pH near 7.5 and $[NO_3^-]_i \approx 1$ mM, with transport coupled to $2H^+$ (Zhen et al., 1991; Miller & Zhen, 1991). That the NO_3^--evoked current failed to cross — or even approach — the voltage axis, is nonetheless a predictable consequence of current subtraction and arises simply because cytoplasmic concentrations of NO_3^- and any putative cotransported ion are likely to be finite and experimental manipulation of adding NO_3^- itself thus affects the thermodynamic constraints on transport (Blatt, 1986). True estimates of the transport current in this case can be obtained by explicit use of the difference current equations, but for practical purposes the δ*I–V* data in these experiments contained negligible subtraction error at voltages near and negative to −100 mV (Blatt, 1986). These points have been developed previously (Meharg & Blatt, 1995) and are addressed in the Discussion.

Charge Stoichiometry for NO_3^- Transport

Data such as shown in Fig. 3 can be related directly to conventional flux measurements of net (chemical) ion uptake, and these were carried out in parallel experiments. Chemical flux measurements are necessarily obtained without control of the membrane voltage, so comparisons were based on difference currents calculated at the free-running membrane potential in the presence of NO_3^-. Net uptake of the anion was recorded using extracellular macroelectrodes to follow the time course of NO_3^- depletion from liquid suspension cultures in K^+/Ca^{2+}-MES, pH 6.1 after stepwise additions of NO_3^- to the suspensions, and chemical flux was calculated from the rate of depletion to 90% of the initial NO_3^- concentration added, correcting for background NO_3^- efflux as recorded in the absence of added NO_3^- and, following exposures to 100 μM NO_3^-, after washing and resuspending the cells in fresh buffer without NO_3^-.

Figure 4 summarizes the results of parallel measurements in 6 independent experiments, including voltage clamp data from 23 cells, calculated on a common basis of cell surface area. The data for net chemical uptake are shown together with the curve for the best fitting to a simple hyperbolic (Michaelis-Menten) saturation function. The data yielded a K_m of 23 ± 4 μM and J_{max} of 72 ± 6 pmol $cm^{-2}sec^{-1}$ for the chemical uptake. Measurements of δI_{NO_3}, determined at the free-running membrane potential in NO_3^-, closely followed the chemical flux. Separate fittings to the current data gave values statistically indistinguishable from the chemical uptake measurements. For the current, the K_m and J_{max} values were 27 ± 4 μM and 86 ± 5 peq $cm^{-2}sec^{-1}$, respectively.

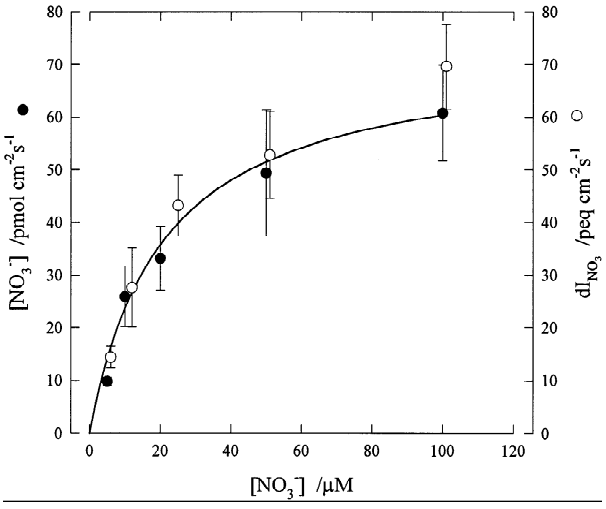

Fig. 4. Equivalence of NO_3^- transport current and net (chemical) NO_3^- uptake rate in *Neurospora* at the free-running membrane potential. Currents (○) in units of peq $cm^{-2}sec^{-1}$ determined as δI_{NO_3} at the free-running membrane potential in the presence of NO_3^-. Net uptake rate (●) calculated from the initial rate of NO_3^- depletion from the bath following additions (*see* Fig. 5). Current data were pooled from 34 cells; Uptake measurements were from 6 independent experiments. Data shown are means ± SE. The solid curve is the result of nonlinear least-squares fitting of the uptake data to a hyperbolic tangent (Michaelis) function. Fitting parameters: K_m, 23 ± 4 μM; J_{max}, 72 ± 6 pmol $cm^{-2}sec^{-1}$. Comparable data were obtained for δI_{NO_3}, yielding parameters: K_m, 27 ± 4 μM; δI_{max}, 86 ± 5 peq $cm^{-2}sec^{-1}$.

Since NO_3^- flux was recorded as net uptake, one caveat to these measurements is that a significant NO_3^- efflux could give falsely low measure of (chemical) NO_3^- uptake. In that case, the fraction of coupled charge influx would be reduced, conceivably even to zero. Unidirectional flux measurements are not straightforward for NO_3^- (Lee & Clarkson, 1986). Nonetheless, a significant contribution of NO_3^- efflux to the net uptake measurements can be discounted for at least three reasons: (i) measurements of background $[NO_3^-]_o$ in the absence of added NO_3^- (*not shown*) failed to show any measureable NO_3^- efflux either before or, most significantly, after 10-min exposure to 100 μM NO_3^-; (ii) an estimation of the possible rise in $[NO_3^-]_i$ under these conditions, assuming an uptake rate of 50 pmol $cm^{-2}sec^{-1}$ and an initial $[NO_3^-]_i$ of zero, shows that it could require 20 min or more to achieve cytoplasmic concentrations of NO_3^- typical of N-replete cells (Zhen et al., 1991; Miller & Zhen, 1991; King, Siddiqi & Glass, 1992); finally, (iii) membrane depolarizations and increases in membrane conductance associated with a time-dependent build-up of cytoplasmic anion concentration (Blatt & Slayman, 1983) were not observed in these experiments (*cf.* Fig. 1). Indeed, even if it is assumed that NO_3^- efflux accounted for approximately 20% of the uptake measured in the N-starved tissue (Deane-Drummond & Glass, 1983*a;* Lee & Clarkson, 1986*a*), the difference would not significantly alter the relationship apparent between the chemical flux and current in the data of Fig. 4. For similar reasons — and because ClO_4^- proved to be a very poor substitute for NO_3^- in electrical measurements (*not shown*) — we question arguments (Deane-Drummond & Glass, 1983a,b; Deane-Drummond, 1985) that NO_3^- uptake may be regulated by control of passive efflux rather than modulation of the uptake process itself.

In addition, experiments were carried out to relate NO_3^- uptake with H^+ movements across the plasma membrane. In *Neurospora* the H^+-ATPase predominates charge balance during nutrient transport (Gradmann et al., 1978; Slayman et al., 1994); however, the net effect of H^+ movement on pH_o must ultimately depend on the H^+ balance associated with the current flux between nutrient transport and the H^+-ATPase. So it was anticipated that NO_3^- transport should be paralleled by a comparable uptake of H^+, assuming that NO_3^- uptake was coupled with $2H^+$ and balanced by 1 H^+ via the H^+-ATPase.

For these measurements N-starved suspension culture cells were used after induction for NO_3^- transport as before, but were resuspended in 0.5 mM K^+/Ca^{2+}-MES buffer with added K_2SO_4 and $CaSO_4$ and adjusted to pH 5.5 (*see* Material and Methods) to minimize interference from dissolved CO_2. External pH was recorded with a semi-micro pH combination electrode. The results of one of three experiments in Fig. 5 are shown with the $[NO_3^-]$ scale extended at a constant slope based on concentrations above 10 μM and therefore indicate an apparent $[NO_3^-]_o$ of approx. 5 μM in the absence of NO_3^-. Measurements were initiated by additions of 1,000 and then 500 nmol NO_3^- to the suspension (upward step of NO_3^--electrode signal) and show that the subsequent disappearance of NO_3^- from the bath was accompanied by an alkalinization of the bath. The initial pH_o was recovered on addition of 1,500 nmol HCl at the end of the experiment. Similar results were obtained in each experiment, giving a mean ratio of NO_3^-:H^+ based on net uptake of 1.08 ± 0.7 and, taken together with the data in Fig. 4, imply a charge-coupling stoichiometry of 1:1 and with $2H^+$:$1NO_3^-$ transported.[1]

[1] It may be argued, by analogy with the comparative NO_3^- flux and electrical measurements of Fig. 4, that these data do not take account of charge balance via K^+ in addition to H^+ efflux (Eddy & Hopkins, 1985). However, previous work has shown that that under nutrient starvation — when membrane voltage is high — K^+ does not play a significant part in charge balance (Rodriguez-Navarro et al., 1986). Indeed, in these experiments, even NO_3^- additions of 0.1 mM still left V_m well-negative (*see* Figs. 1 and 3) of any reasonable value for E_k [approx. −100 mV in 2 mM K^+ for $[K^+]_i \approx 150$ mM (Slayman & Tatum, 1968; Rodriguez-Navarro et al., 1986)]. So, the driving force for K^+ flux would still be inward and a passive K^+ efflux could not account for the outward current balancing NO_3^- uptake.

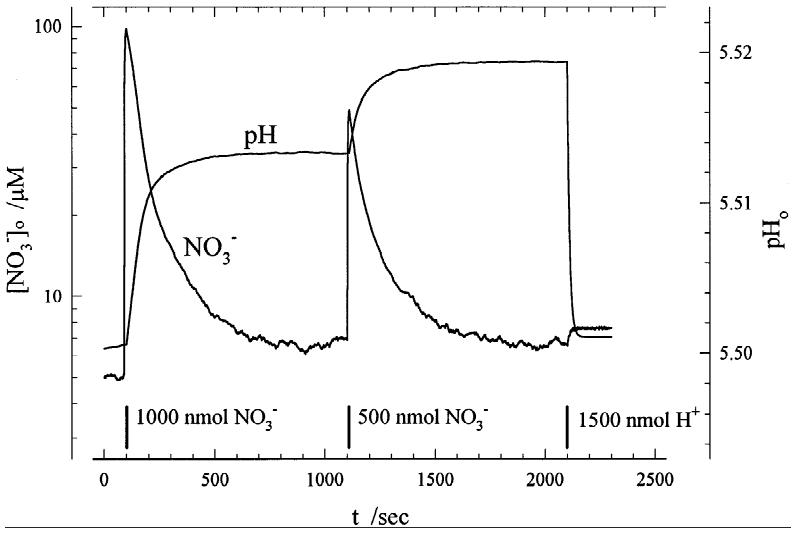

Fig. 5. Equivalence of net (chemical) NO_3^- and H^+ uptake in simultaneous recordings of $[NO_3^-]_o$ and pH_o bathing *Neurospora* suspension culture cells. Measurements carried out after induction for NO_3^- transport and resuspension in 0.5 mM K^+/Ca^{2+}-MES buffer at pH 5.5 with K_2SO_4 and $CaSO_4$ added (final $[K^+]$ = 2 mM, $[Ca^{2+}]$ = 1 mM). External pH was recorded with a semi-micro pH combination electrode with Cl^- omitted from the reference. The $[NO_3^-]$ scale shown is extended from the slope at concentrations above 10 μM and therefore indicates an apparent $[NO_3^-]_o$ of approx. 5 μM in the absence of NO_3^-. Measurements were initiated by additions of 1,000 nmol, and then 500 nmol NO_3^- to the suspension (upward steps of NO_3^--electrode signal) and disappearance of NO_3^- and H^+ from the bath followed over time. Titration of the pH with HCl thereafter indicated a NO_3^-:H^+ uptake ratio of 1.04 based on net uptake and of 1.02 based on initial uptake rate. Similar results were obtained in two other experiments.

NO_3^--Transport Current is Unaffected by Metabolic Blockade or NH_4^+

The arguments favoring energization by ion-coupling aside, NO_3^- in *Neurospora* (Schloemer & Garrett, 1974) — as in higher plants (Heimer & Filner, 1970; Rao & Rains, 1976; Glass et al., 1990) — is acutely sensitive to metabolic poisons and uncouplers which might suggest a more immediate link to ATP and metabolic energy output. However, these, and additional observations of short-term metabolite repression or competition (Rao & Rains, 1976; Breteler & Nissen, 1982; Deane-Drummond & Glass, 1982; Ullrich et al., 1984; Deane-Drummond, 1985; Ullrich & Novacky, 1990; Hawkins & Lewis, 1993) might also be understood as an effect mediated through changes in membrane voltage and a corresponding kinetic restriction on uptake, given the voltage dependence of the NO_3^- current (Fig. 3). Indeed, similar patterns of behavior are well-known for ion-driven transporters, notably for H^+-coupled K^+ transport in *Neurospora* (Blatt et al., 1987), that exhibit profound kinetic dependencies on membrane voltage.

To explore the effect of metabolic blockade systematically, we carried out a series of voltage-clamp experiments of the type shown in Fig. 3, reasoning that if NO_3^- transport depended primarily on membrane voltage — and so, only indirectly on ATP hydrolysis — then under voltage clamp the NO_3^- transport current should be unaffected by metabolic poisons. The data in Fig. 6 are from one cell and show that metabolic blockade led to an extensive and rapid depolarization of the membrane voltage, from −245 mV to a stable value around −100 mV (Fig. 6*A*, *inset*). In this experiment, prior addition of NO_3^- evoked an approx. +30 mV shift in V_m from −234 mV to a value close to −200 mV; however, in the presence of NaCN and SHAM a second challenge with NO_3^- gave less than a +10 mV change in V_m. Voltage-clamp recordings obtained in the absence of NO_3^- (○,□) yielded characteristics typical of H^+-ATPase inhibition by ATP withdrawal in cyanide (Slayman et al., 1994; Gradmann et al., 1978), including a marked reduction in membrane conductance most notable at voltages negative of approx. −100 mV. Comparison of voltage-clamp data gathered immediately prior to, and during the first exposure to NO_3^- (○, ●) showed the familiar downward shift of the *I–V* curve in NO_3^- (Fig. 6*A*). Significantly, a second challenge with NO_3^- carried out in the presence of NaCN and SHAM evoked a similar pattern of response in the current characteristic (□, ■), with NO_3^- addition leading to a downward shift in membrane current that was most prominent at more negative-going voltages (Fig. 6*A*). Current subtractions (Fig. 6*B*) confirmed this minimal effect on NO_3^- transport current, demonstrating only a small reduction in the magnitude of δI_{NO_3} at any one voltage. Thus, despite the considerable change in membrane conductance and the shape of the whole-cell *I–V* relations under metabolic blockade, the effect on the NO_3^- δ*I–V* curve was small and limited essentially to a change in amplitude. These features of the NO_3^- current, and their juxtaposition with inhibitor action on the background of membrane currents, argue in favor of an indirect action mediated through a reduction in electrical driving force.

A similar conclusion was drawn from studies with the NO_3^- metabolite NH_4^+. In these experiments, fully induced hyphae were challenged with 100 μM NO_3^- in the absence, and again in the presence of 0.1–0.5 mM NH_4^+. Figure 7 shows the results from one experiment with 0.1 mM NH_4^+, close to the K_i reported for inhibition of NO_3^- uptake (Schloemer & Garrett, 1974). In this

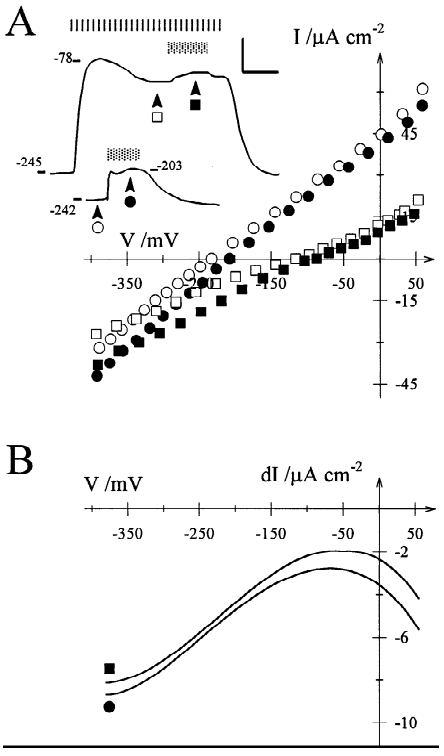

Fig. 6. NO_3^- transport current in *Neurospora* persists in the presence of metabolic blockade with NaCN and salicylhydroxamic acid. Steady-state current-voltage (*I–V*) and difference-current-voltage (δ*I–V*) curves obtained from one *Neurospora* hypha before and during exposure to 1 mM NaCN and 0.4 mM salicylhydroxamic acid. (*A*) *I–V* curves determined at time points before (○) and during (●) exposure to 100 μM NO_3^- in the absence of the metabolic poisons, in their presence (□) and after further addition of 100 μM NO_3^- (■). *Inset:* Free-running membrane potential traces with voltages indicated in mV. Carats indicate times of *I–V* scans (masked from trace) and cross-referenced by symbol. Scale: vertical, 50 mV; horizontal, 3 min. Vertical shaded bar indicates exposure period for NaCN + salicylhydroxamic acid; stripped bars indicate exposure periods for NO_3^-. *B* δ*I–V* curves for NO_3^- transport recorded during NO_3^- exposure, before (●) and during metabolic blockade (■). Note the different current scale from *A*.

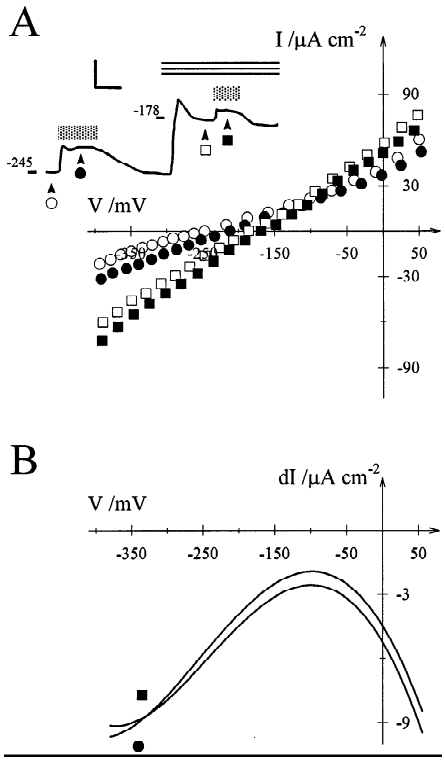

Fig. 7. Ammonium blocks NO_3^- transport current of fully induced *Neurospora* hyphae through membrane depolarization without altering the intrinsic kinetic characteristics of the current. Data from one hypha in 10 mM K^+/Ca^{2+}-MES pH 6.1, challenged with 100 μM NO_3^- in the absence, and presence of 100 μM NH_4^+. (*A*) Whole-cell, steady-state *I–V* scans carried out ± NO_3^- before (○, ●) and after (□, ■) adding NH_4^+. *Inset:* Membrane voltage trace, voltages indicated in mV. Additions of NH_4^+ (stippled bars) and NH_4^+ (horizontal-striped bar) indicated above. Carats mark times of *I–V* scans (masked from trace), cross-referenced to *I–V* curves by symbol. Scale: vertical, 40 mV; horizontal, 3 min. (*B*) NO_3^- transport current, δI_{NO_3}, derived by current subtractions of the whole-cell currents ± NO_3^- in *A* and cross-referenced by symbol.

case, the hypha was challenged with 100 μM NO_3^- first alone, and subsequently in the presence of NH_4^+. Adding NO_3^- on its own resulted in a membrane depolarization of +38 mV (Fig. 7*A*, *inset*) and downward shift in the whole-cell *I–V* curve (Fig. 7*A*, compare curves ○ and ●) which, on current subtraction, yielded the characteristic NO_3^- current (Fig. 7*B*). Adding NH_4^+, following NO_3^- washout, evoked a much larger inward current and consequent depolarization (Slayman, 1977), marked in the whole-cell *I–V* curve by an approx. 3-fold increase in slope (conductance) across the accessible voltage spectrum [compare *I–V* curves in the absence of NO_3^- (○,□)]. Against this added background conductance, the depolarization on the second addition of NO_3^- was reduced to +12 mV. Furthermore, a 31% reduction of NO_3^- uptake was also indicated under free-running (nonvoltage-clamp conditions) in the presence of NH_4^+. However, current subtraction over the entire range of clamp voltages showed virtually no change in the NO_3^- δ*I–V* characteristic (Fig. 7*B*). Similar results were obtained in 4 other experiments and gave a mean inhibition by NH_4^+ of 32 ± 5% at the free-running voltage, a value close to the 25% reduction observed by Schloemer and Garrett (1974) in uptake measurements carried out on (nonvoltage-clamped) *Neurospora* in suspension cultures. However, at a standard clamp voltage of −200 mV the NO_3^- current in NH_4^+ was 102 ± 6% of that recorded in the control. In other words, NH_4^+ inhibition of the NO_3^- current could be accounted for entirely as a consequence of membrane depolarization.

Kinetic Interaction of $[NO_3^-]_o$, $[H^+]_o$ and V_m

From the preceding experiments it is evident that any measurement of NO_3^- transport — whether as a differ-

ence current $\pm NO_3^-$, net or isotopic (unidirectional) flux — will be influenced by five kinetic variables: $[NO_3^-]_o$, $[NO_3^-]_i$, V_m and, assuming cotransport with H^+, also $[H^+]_o$ and $[H^+]_i$. Only two of these variables, $[NO_3^-]_o$ and $[H^+]_o$, are controlled in flux experiments when measurements are carried out without clamping the membrane voltage. The intracellular concentrations may be assumed to be constant, provided that the experiments are short-term and the initial rates of transport are used in quantitation. However, unless V_m is brought under experimental control using a voltage clamp, the resulting kinetic detail will not be sufficient for a comprehensive modelling of the transport process, especially given that NO_3^- transport is voltage sensitive over the normal physiological voltage range (Figs. 3 and 6).

Our previous studies of *Arabidopsis* root hairs demonstrated the facility of the electrophysiological approach for analysing high-affinity NO_3^- transport (Meharg & Blatt, 1995), and a comparison with the features of the NO_3^- current in *Neurospora* (*cf.* Figs. 3 and 6) underscored some similarities in the voltage sensitivities of the currents. Thus, one objective of the present experiments was to develop an explicit kinetic model for the transporter in *Neurospora* and to place this model in context with the that for NO_3^- transport in *Arabidopsis.* To obtain the broadest range of data for modelling, experiments were carried out similar to those illustrated in Figs. 3 and 6, but varying both extracellular NO_3^- and pH. Analyses were generally restricted, however, to comparing currents recorded from the same cell in order to accommodate variations in current magnitudes between measurements (up to 2-fold on a cell-by-cell basis). The possibility of changes in pH_i and $[NO_3^-]_i$ was minimized by limiting NO_3^- exposures to short pulses, just long enough to encompass full membrane depolarization (*see* Fig. 3), and control measurements were run under a set of standard conditions for $[NO_3^-]_o$ and pH_o throughout each set of measurements as a check against any endogenous variation or kinetic adaptation during a sequence of NO_3^- challenges.

The simplest result to describe was that of the difference current δI_{NO_3} at a fixed $[NO_3^-]_o$ and V_m. The results shown in Fig. 8 were carried out with additions of 100 μM NO_3^- and were pooled from 5 cells after normalizing to measurements in pH_o 5.5. The data show that the current was enhanced at acid pH_o, with an apparent maximum near pH_o 5.5–6.0. Also consistent with a kinetic dependence on H^+, exposing *Neurospora* hyphae to 10 mM Na^+-butyrate, sufficient to acidify the cytoplasmic pH approx. 0.5 units (Sanders & Slayman, 1982), reduced the NO_3^- current by 30–40% at all clamp voltages (Fig. 9).

For reasons discussed later, the most useful information was to be obtained at the kinetic extremes, under conditions of near-saturating $[H^+]_o$, $[NO_3^-]_o$ and saturating (negative) V_m. A more detailed presentation of the

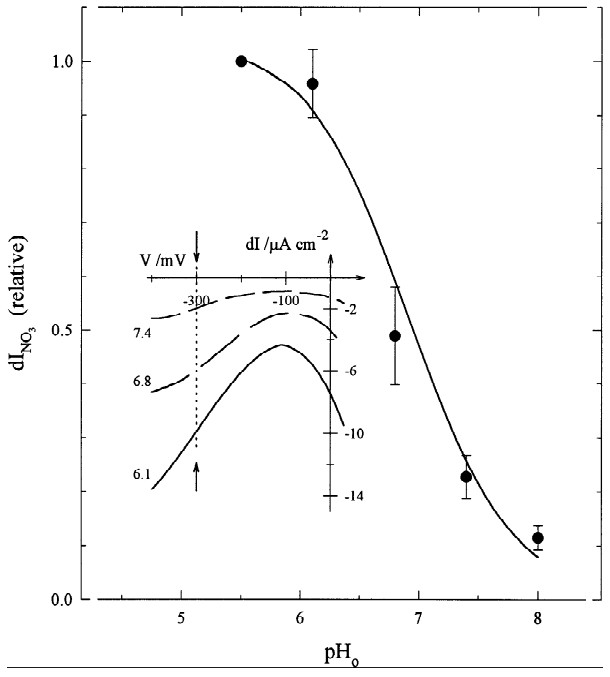

Fig. 8. Extracellular pH affects the NO_3^--evoked current in *Neurospora* independent of changes in membrane voltage. Difference currents calculated for 100 μM NO_3^- exposures with the membrane clamped to −300 mV (*see insert*). Data are pooled from 6 experiments, with difference currents normalized to common measurements at pH_o 5.5 from each cell. The data were fitted by least-squares to the Henderson-Hasselbalch equation (solid line), which yielded an apparent pK_a of 6.92 ± 0.05. *Inset:* Difference-current-voltage (δI–V) curves as a function of H^+ concentration in the bath. Data from one *Neurospora* hypha challenged with 100 μmM NO_3^-. Curves are for NO_3^- exposure at pH_o 6.1 (solid line), pH_o 6.8 (long dashed line) and pH_o 7.4 (short dashed line). Values taken at −300 mV indicated by vertical dotted line and arrows. pH values indicated on left.

effect of extracellular pH is given in Fig. 10*A.* For the analyses shown, values of the NO_3^- difference current, δI_{NO_3}, were recorded from one cell near the negative voltage extreme (−350 mV) and at each of three different pH_o values, and then subjected to nonlinear least-squares fitting to a Michaelis function with $[NO_3^-]_o$. As seen, both Michaelis parameters K_m and $\delta I_{NO_3,max}$, derived from this analysis, were altered by pH_o consistent with its behavior as a ''linear mixed-type activator'' (Segel, 1993): increasing $[H^+]_o$ from 0.16 to 3.2 μM (from pH_o 6.8 to 5.5) caused a limited increase in $\delta I_{NO_3,max}$, but showed a substantial effect on the K_m for NO_3^- which decreased, consistent with a *ca.* 4-fold rise in affinity for NO_3^-. Hence the current, like net NO_3^- uptake (Schloemer & Garrett, 1974; Rao & Rains, 1976), was reduced at alkaline pH_o, but in this case the effect was demonstrably independent of any effect of pH_o on the membrane voltage.

Previous studies (Sanders et al., 1984; Blatt, 1986; Blatt et al., 1987; McCulloch et al., 1990; Slayman et al.,

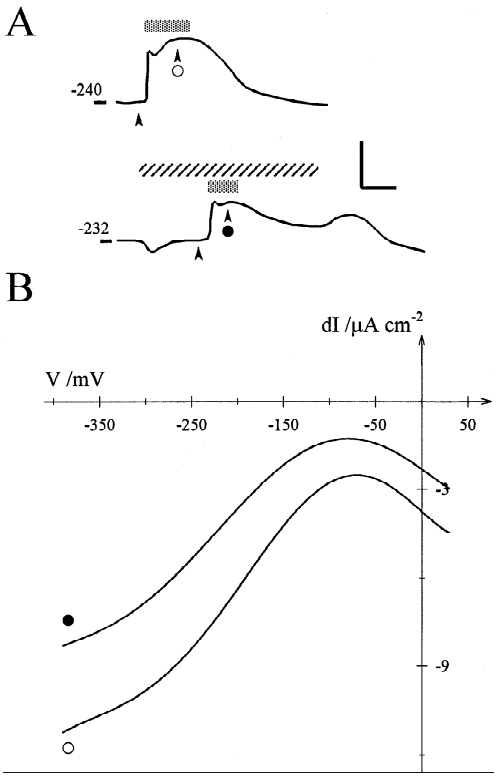

Fig. 9. Intracellular pH affects the NO_3^--evoked current in *Neurospora* independent of changes in membrane voltage. Membrane voltage response (*A*) and difference currents (*B*) determined for 100 μM NO_3^- exposures in one hyphae in the absence (○) and presence (●) of intracellular H^+ load from 10 mM Na^+-butyrate added at pH_o 6.1. (*A*) Voltage traces (in mV on left) with periods of exposure to 100 μM NO_3^- (stippled bars), 10 mM Na^+-butyrate (diagonally-striped bar), and times of *I–V* scans (carats, cross-referenced to *B* by symbol) indicated. Scale: vertical, 50 mV; horizontal, 3 min. H^+ loading and its effect on H^+-ATPase and background leak conductances (*not shown*) account for the transients on Na^+-butyrate addition and washout (Sanders & Slayman, 1982). (*B*) Difference-current characteristics determined as in Fig. 3 from measurements in the absence (○) and presence (●) of intracellular H^+ load from 10 mM Na^+-butyrate. Comparable results were obtained in 3 additional experiments.

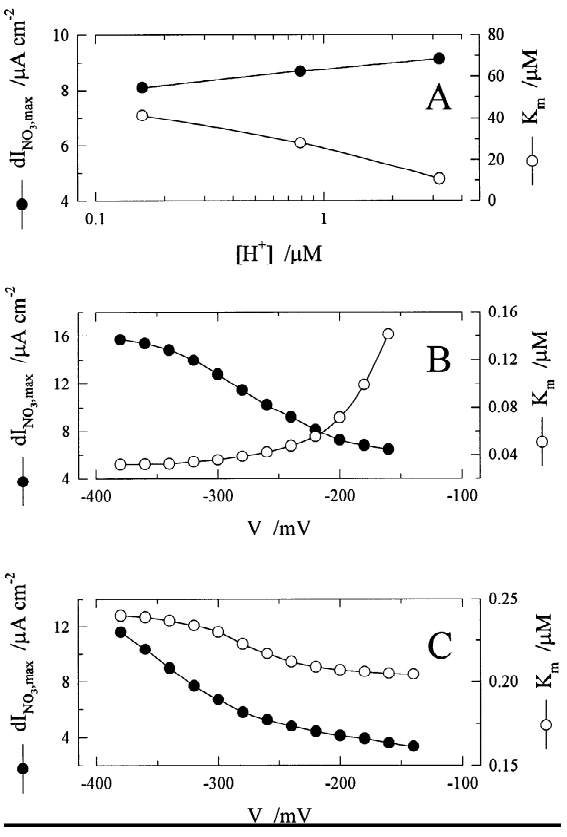

Fig. 10. Kinetic interaction between parameters of $[NO_3^-]_o$, $[H^+]_o$ and membrane voltage in *Neurospora*. (*A*) Proton concentration-dependence of the kinetic parameters (δI_{max}, K_m) for δI_{NO_3} at extreme negative voltage. Currents determined at −350 mV as described in Fig. 3 at $[NO_3^-]_o$ between 6 and 100 μM and fitted by nonlinear least-squares (Marquardt, 1963) to a Michaelis function. The parameters resulting from this and similar analyses at three different pH_o values are plotted as a function of $[H^+]_o$. (*B*) Voltage dependence of kinetic parameters (δI_{max}, K_m) for δI_{NO_3} at pH_o 6.1. Results derived from analyses as in (*A*), but as a function of clamp voltage. (*C*) Voltage dependence of kinetic parameters (δI_{max}, K_m) for δI_{NO_3} at 200 μM $[NO_3^-]_o$. Results derived from analyses as in *B*, but for $[H^+]_o$ as a function of clamp voltage.

1994) have indicated that, in discriminating between alternative reaction cycle models, the influence of membrane voltage on transport kinetics is often more informative than the effects of changing either substrate or driver-ion (H^+) concentrations. Therefore, kinetic analyses were also carried out to examine the effects of V_m on transport first with $[NO_3^-]_o$ and then with $[H^+]_o$ as the primary variable. Figure 10*B* summarizes the effect of V_m on K_m and $\delta I_{NO_3,max}$ for $[NO_3^-]_o$. These measurements were carried out at near-saturating pH_o (5.5) with $[NO_3^-]_o$ as the independent variable. Figure 10*C* shows the results of comparable measurements, but carried out at near-saturating $[NO_3^-]_o$ (200 μM) with $[H^+]_o$ as the independent variable. In each of these cases, values of δI_{NO_3} were determined in turn at one of several common clamp voltages and used to construct families of Michaelis plots as functions either of $[NO_3^-]_o$ or $[H^+]_o$ as before.

The Michaelis parameters derived from these analyses show that the action of membrane voltage over $[NO_3^-]_o$, again, was distributed between the maximum current and the apparent affinity of the transporter for NO_3^-. Increasing-negative V_m, like $[H^+]_o$, acted as a ''linear mixed-type activator'' (Segel, 1993) of transport with respect to NO_3^- concentration, and between approx. −150 and −350 mV led to a 4-fold increase in δI_{max} and an approx. 3-fold decrease in K_m. By contrast, with respect to $[H^+]_o$ (pH_o varied between 5.5 and 7.4) the analyses uncovered a parallel action of V_m on δI_{max} and K_m (Fig.

$10C)^2$. In this case, increasing the electrical driving force across the membrane effected a rise in the maximum transport current. It also consistently led to a small decrease in the apparent affinity of the transporter for H^+. This latter, and counter-intuitive result implicated the rate-limiting H^+-binding step at a position in the transport cycle that is kinetically remote from membrane charge transit. The juxtaposition of these observations, and their relation to the characteristics for NO_3^- transport in *Arabidopsis* (Meharg & Blatt, 1995), prompted the examination of ordered binding models presented below.

Discussion

High-affinity NO_3^- transport in fungi, as in higher-plants and algae, is energetically unfavorable and requires that the cells draw upon a metabolic input to achieve NO_3^- uptake. The consensus holds that NO_3^- transport is coupled to the primary electrochemical potential gradient for H^+ ($\Delta\mu_H$) in walled eukaryotic cells. Nonetheless, the significance of membrane depolarizations upon addition of NO_3^- — their implications for metabolic dependence, competing ion and inhibitor sensitivities — has remained only poorly defined, and evidence that could speak directly to the charge-coupling ratio for NO_3^- transport or its dependence on $\Delta\mu_H$ has generally remained elusive.

The results presented here, and our previous studies with *Arabidopsis* root hairs (Meharg & Blatt, 1995), highlight the common and pivotal role of the voltage parameter in dictating the kinetic characteristics for NO_3^- transport. For *Neurospora*, voltage clamp recordings identified a marked dependence of the NO_3^- current on membrane potential (Figs. 3 and 6–9), and exposed the sensitivity of the current to pH_i and pH_o distinct from pH-dependent changes in V_m (Figs. 8 and 9). Finally, comparative flux and electrical measurements yielded a 1(+):1(NO_3^-) charge-coupling stoichiometry for uptake, indicating that 2 positive charges must transit the membrane with each NO_3^- anion, and concurrent measurements of net H^+ and NO_3^- transport showed that uptake at micromolar NO_3^- concentrations was accompanied by a net influx of roughly an equivalent number of H^+. Given that the dominant pathway for charge efflux balancing noncapacitative, inward-directed currents is the H^+-ATPase (Slayman & Gradmann, 1975; Slayman et al., 1994) taken together these results offer a compelling argument for the transport of NO_3^- coupled with the movement of $2H^+$.

Kinetic Dependence on Membrane Voltage

Although in principle voltage sensitivity is a common feature of all rheogenic transport processes, high-affinity NO_3^- transport — in *Neurospora* as in *Arabidopsis* (Meharg & Blatt, 1995) — is unusual among anion transporters as it is for H^+-coupled transport processes generally — simply because its region of steep voltage dependence is situated within the normal range of physiological membrane potentials. In most other H^+-coupled systems known to date transport currents have appeared largely voltage-insensitive (Hansen & Slayman, 1978; Felle, 1981; Beilby & Walker, 1981; Sanders & Hansen, 1981; Sanders et al., 1983), consistent with equilibrium potentials situated well-positive of these potentials [but *see* (Blatt, 1986)]. An important consequence for NO_3^- transport in *Neurospora* is that uptake of the anion will be strongly influenced by factors which affect the free-running membrane voltage. From Figs. 3, 6 and 7 it is clear that shifting the membrane positive-going from −300 to −150 mV can reduce the NO_3^- current by 50–70% under constant $[NO_3^-]_o$ and pH_o.

One consequence of this voltage dependence is that factors that influence the free-running membrane potential must thereby also affect NO_3^- uptake, albeit indirectly. It is precisely this ''functional coupling'' that probably accounts for the sensitivity of NO_3^- transport to metabolic poisoning with cyanide (Glass et al., 1990; Schloemer & Garrett, 1974; Rao & Rains, 1976). Treatment with NaCN and salicylhydroxamic acid led to a pronounced depolarization of the *Neurospora* membrane but had little effect on the NO_3^- current, as could be demonstrated when the voltage clamp was used to ''maintain'' the membrane potential (Fig. 6). Much the same conclusion can be drawn from experiments with NH_4^+ (Fig. 7), which has been reported to interfere with NO_3^- uptake (Goldsmith et al., 1973; Deane-Drummond, 1985; Henriksen et al., 1990; Henriksen & Spanswick, 1993), and the explanation should apply equally to the response of NO_3^- uptake to other transported solutes against which the transporter must ''compete'' for the electrical driving force. Indeed, there are reports that ions such as Cl^- (Deane-Drummond & Glass, 1982; Ullrich & Novacky, 1990; Hawkins & Lewis, 1993), Ca^{2+} (Doddema & Telkamp, 1979), and even Na^+ and K^+ (Smith, 1973; Jackson et al., 1976; Eddy & Hopkins, 1985; Hawkins & Lewis, 1993) interact with NO_3^- transport or regulate its activity. Yet these solutes, equally, will influence the membrane potential in their transport thereby affecting NO_3^- uptake accordingly — but by virtue of its inherent kinetic dependence on membrane voltage rather than any direct interaction with the NO_3^- trans-

[2] While it could be supposed that, if coupled with the transport of $2H^+$, the current should follow as a function of $[H^+]_o^2$, empirically better results were obtained when the current was plotted as a simple, rather than as a non-unitary power of driver-ion concentration and the observation is entirely consistent with transport rate limited in only one of the two, putative H^+-binding steps (*see* Discussion).

porter itself. In short, for the transport-competent cells a primary level of control on NO_3^- uptake is probably mediated through its endogenous kinetic dependence on membrane voltage rather than by exogenous regulatory interactions with metabolites.

Kinetic Control and Metabolite Suppression are Separable

By contrast with its kinetic behavior in NH_4^+, the induction of NO_3^- transport showed a profound sensitivity to the metabolite. We found that very short exposures to extracellular NO_3^- were sufficient to trigger induction, and that the process could be suppressed if NH_4^+ was present at the same time. Because the electrical analyses allow us to rule out a low level of NO_3^- transport activity in these instances, and because even a brief exposure to NO_3^- was sufficient to express the transport activity 40 to 80 min later (Figs. 1 and 2), the observations suggest that extracellular NO_3^- must trigger an inductive signal cascade independent of a minimum cytoplasmic NO_3^- concentration. This conclusion also accords with the apparent insensitivity of the induction process to subsequent NO_3^- exposures. Similar interpretations have been suggested by Redinbaugh and Campbell (1991), MacKown and McClure (1988) and Tischner et al. (1993), although the longer inductive exposures to NO_3^- and especially the background of NO_3^- uptake in these previous studies left open a question about the requirement for cytoplasmic NO_3^-. In toto, the data point to a highly concerted signalling sequence regulating NO_3^- transporter expression, distinct from the endogenous kinetic control of transporter activity in the membrane.

Kinetic Distinctions of the Fungal NO_3^- Transporter

The juxtaposition of the NO_3^- currents in *Neurospora* and *Arabidopsis* does raise a question about their underlying kinetic equivalence. Although a broad parallel can be drawn from the voltage-dependence of the NO_3^- currents from the plant and fungal cell types, a careful analysis of the current in *Neurospora* uncovered both quantitative and qualitative differences including, on average, a larger NO_3^- current in the N-starved *Neurospora* and an apparent negative-going shift to its voltage characteristic [Fig. 3; compare with Fig. 5 of Meharg and Blatt (1995)]. Most significant, however, kinetic analyses showed that membrane voltage increased δI_{max} and decreased K_m with respect to H^+ (linear-mixed activator), while affecting both δI_{max} and K_m in parallel with respect to NO_3^- (hyperbolic-mixed activator) in *Arabidopsis*. We could deduce the reverse dependencies for the current in *Neurospora* (Fig. 10) and, hence, suspected that kinetic modelling should yield quite a different picture for the fungal transporter.

Essentially all of the kinetic properties of the NO_3^- transport currents in *Neurospora* and *Arabidopsis* can be described by a common set of cyclic reaction models, and we therefore subjected these data to a similar analysis as before (Meharg & Blatt, 1995). The models were conceived in kinetic terms, and no explicit physical assumptions were made, other than to propose that the transported ions traverse the membrane by reacting with a specific carrier molecule which is, itself, confined to the membrane. Each model was reduced to the minimum number of pseudo first-order reaction steps permitted by the data, without identification a priori of any rate-limiting reaction steps (Gradmann, Kleiber & Hansen, 1987), and the voltage parameter was incorporated in a single reaction step as a symmetric Eyring barrier (Läuger, 1991; Läuger & Stark, 1970) so that

$$k_{12} = k_{12}^o e^{zu/2}$$

and [1a,b]

$$k_{21} = k_{21}^o e^{-zu/2}$$

where u = VF/RT, V is the membrane voltage, and F, R and T have their usual meanings.

The minimal kinetic model that is physically consistent with a cotransport system for NO_3^- and two monovalent co–ions (H^+) comprises eight carrier states and sixteen rate constants which describe the sequential binding of substrate and co–ions on one side of the membrane and their debinding on the other side (*see* Fig. 11). The complete equation associated with this (and any other cyclic) cotransport model takes a general form where the transport current

$$I = -zF \frac{k_{12}|^1M_m| - k_{21}|^2M_m|}{|M_m|} \quad [2]$$

in which I is the current, m is the total number of states explicitly included in the model, $|M_m|$ is the determinant for the characteristic matrix of coefficients for that model, $|^jM_m|$ is the determinant for the adjusted matrix of coefficients excluding the jth state ($j = 1$ or 2, associated with membrane charge transit), the ratio $|^jM_m|/|M_m|$ is the total carrier in the jth state (N_1 or N_2), z is the charge moved per forward turnover of the carrier cycle, and F has its usual meaning.

Selecting a Reaction Scheme

Because it is conceivable for membrane charge transit to occur in association with either the bound or unbound transporter, two variants of the reaction scheme in Fig.

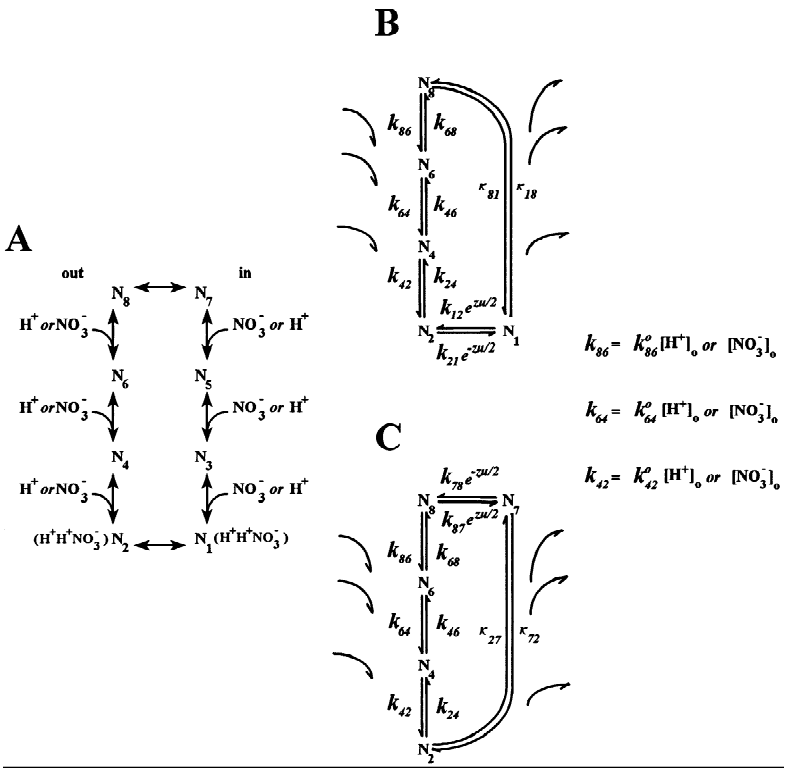

Fig. 11. Carrier cycle for the NO_3^- transporter. Forward operation in each case is in the counter-clockwise direction as illustrated. (*A*) The explicit, eight-state model with all possible binding/debinding orderings for H^+ and NO_3^- indicated. States N_1 and N_2 denote the loaded carrier states on the inside and outside of the membrane, respectively, while states N_7 and N_8 comprise recycling of the unloaded carrier across the membrane. All intervening steps entail binding/debinding of H^+ or NO_3^- inside and outside. (*B*) Model I (*see* text): pseudo-5-state model equivalent with membrane charge transit assigned to the loaded carrier ($z = +1$). (*C*) Model II (*see* text): pseudo-5-state model equivalent with membrane charge transit assigned to the unloaded carrier ($z = -1$).

11*A* must be considered. Model I (Fig. 11*B*) assumes that the transporter itself is uncharged and assigns the charge transit step to the fully loaded arm of the cycle. Model II (Fig. 11*C*) postulates that the unloaded transporter carries a net charge of −1 across the membrane during carrier recycling and that the loaded carrier is electrically neutral. Each model actually entails nine possible reaction cycles, taking into account the different combinations of ordered binding and release, but these sequence permutations are reduced to three in the pseudo five-state (lumped) forms, reflecting the fact that our experiments did not examine the effects of $[NO_3^-]_i$ and $[H^+]_i$ in quantitative terms and can provide no information about ion binding inside the cell. The corresponding reaction cycles are shown on the right in Fig. 11 and follow the conventions of Hansen et al. (1981), Sanders et al. (1984), Blatt (1986) and Gradmann et al. (1987) where the *k*s denote simple reaction constants and the κs indicate the lumped constants that subsume multiple steps. Reaction constants which contain ion-concentration terms are expanded at the far right in Fig. 11. Thus, each model may be further subdivided depending on the order of binding outside, that is either with the binding of NO_3^- first [Models I(F) and II(F)], last [Models I(L) and II(L)], or mid between the two H^+ binding steps [Models I(M) and II(M)].

For both Models I and II, all of the matrices in Eq. 2 and its congeners represent linear combinations of the reaction constants. Many of the terms in the numerator cancel, but the general expression is non-Michaelian except under certain, well-defined circumstances, notably when the transport difference current δI is calculated (Blatt, 1986; Blatt et al., 1987). Each equation includes terms in $[NO_3^-]_o$, $[H^+]_o$ and V, and further simplifies when saturating conditions in each of these parameters are considered in turn. The resulting subfamilies of equations include a single product term in the numerator and terms in the denominator which factor to give a sum of products in the substrate (or co-ion) concentration termed and a second sum of products in a constant term. Thus Model I(L), with NO_3^- binding last before membrane charge transit, reduces to

$$\frac{I}{-FN} = \frac{k^o_{42}[NO_3^-]_o k^o_{21} e^{-u/2}\,\kappa_{18}}{k^o_{42}[NO_3^-]_o(k^o_{12}e^{u/2} + k^o_{21}e^{-u/2} + \kappa_{18}) + \kappa_{24}k^o_{12}e^{u/2} + \kappa_{18}k^o_{21}e^{-u/2}} \quad [3]$$

and, after minor rearrangement of terms, gives the Michaelis parameters

$$\frac{I_{max}}{-FN} = \frac{k^o_{21}e^{-u/2}\kappa_{18}}{k^o_{21}e^{u/2} + k^o_{21}e^{-u/2} + \kappa_{18}} \quad [4a]$$

$$K_m = \frac{k^o_{12}e^{u/2}\kappa_{24} + k^o_{21}e^{-u/2}\,\kappa_{18}}{k^o_{12}e^{u/2} + k^o_{21}e^{-u/2} + \kappa_{18}} \quad [4b]$$

A complete summary of the relevant equations and Mi-

chaelis parameters for saturating substrate and co-ion concentration will be found in Meharg and Blatt (1995, Table 2). For comparison with the models depicted in Fig. 11, forward operation of the transporter occurs in the counter-clockwise direction. Note that the data in Fig. 10*A* probably do not satisfy the limiting condition of saturating negative membrane voltage, and were therefore given less weight in this analysis. Also, as in the case of *Arabidopsis* (Meharg & Blatt, 1995), functions in $[H^+]_o$ were potentially non-Michaelian, simply because H^+ binding was necessarily assigned to two steps. The equations become Michaelian in $[H^+]_o$ when the reaction constant for reverse (clockwise) transit through one of these steps is very small. In keeping with the apparent Michaelian behavior of the data we incorporated this assumption, thereafter including the ''missing'' reaction constants in the size orderings as appropriate.

Identifying Kinetically Consistent Models

Within the limiting conditions stipulated for two of the families of equations derived from Eq 2, each set of data in Fig. 10 describes Michaelian parameters δI_{max} and K_m, determined either in $[NO_3^-]_o$, $[H^+]_o$, or membrane voltage. Thus, the problem of discriminating between the models in Fig. 11 reduced to one of finding a single set of conditions, defined by the predicted size ordering of reaction constants which are internally consistent and which satisfy the pattern of δI_{max} and K_m behavior in Fig. 10, that is which predict an increase and/or decrease in each of the parameters with voltage under each of the limiting conditions.

Examining the parameter equations (Meharg & Blatt, 1995) shows that both of the models in all binding order combinations will account for the data in Fig. 10. In every case, orderings of reaction constants can be found which give a parallel increase of δI_{max} and K_m as functions in $[H^+]$ with increasing (negative) membrane voltage. However, only Models I(L) and II(F) — both with NO_3^- binding adjacent to the charge transfer step across the membrane — give combinations of reaction constants for which K_m may decrease with (negative) membrane voltage consistent with Fig. 10*B*. Of these, only model II(F) satisfies the experimental data without internal inconsistencies. Model I(L), by contrast, requires that $k^o_{21} >> k^o_{12}$, κ_{18} for K_m to decrease with increasing negative voltage, but dictates orderings with $\kappa_{18} > k^o_{21} > k^o_{12}$ or $k^o_{21} >> k^o_{12}$, κ_{18} for I_{max} to increase under the same conditions [Table 2 columns 2 and 3, rows 8 and 9; (Meharg & Blatt, 1995)]. Taking account of all reaction constant orderings entailed by the data of Fig. 10 in conjunction with the several Michaelis parameter equations gives the minimal overall ordering

$$\kappa_{27} >> \kappa_{72} > k^o_{87}e^{u/2} > k^o_{78}e^{-u/2},\ k_{24} >> k_{46} \qquad [5]$$

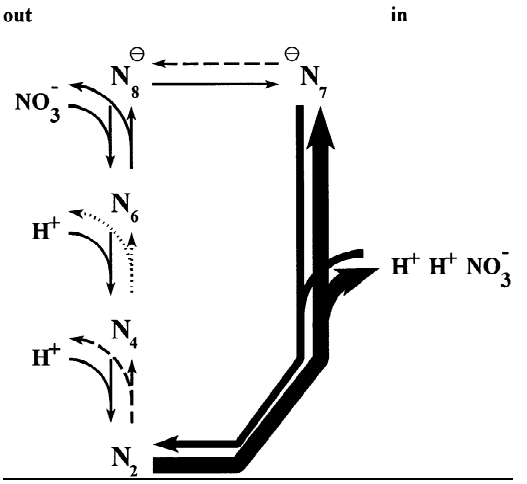

Fig. 12. Reaction kinetic cycle for the *Neurospora* NO_3^- transporter. Line weights drawn to convey the relative magnitudes for the reaction constants. Key features are: (i) overall rate limitation in the forward (counter-clockwise) direction by membrane transit of the charged (unloaded) carrier (reaction constant k^o_{78}); (ii) rate dominance of the binding/debinding steps inside the cell, determined by the lump constants κ_{27} and κ_{72}; (iii) kinetic proximity of NO_3^- and rate-limiting H^+ binding steps outside to membrane charge transit; (iv) kinetic isolation of NO_3^- and rate-limiting H^+ binding steps outside from each other. Details in the text.

which is summarized schematically in Fig. 12 with the relative size ordering of reaction constants indicated by the line weight of the arrows.

Implications of the Model and Comparison with NO_3^- Transport in Arabidopsis

The characteristics of the model in Fig. 12 highlight several prominent features which, despite obvious differences to the NO_3^- transporter of *Arabidopsis*, mark the close kinetic juxtaposition of the two transport processes:

(i) Like the *Arabidopsis* system, the *Neurospora* transporter is predicted to carry a net negative charge in its unloaded form; overall balance of the rate-dominant and rate-limiting reaction steps is weighted in favor of the loaded (uncharged) carrier outside and rapid equilibration with the unloaded carrier inside the membrane; and, in the forward (counter-clockwise) direction, membrane transit of the charged (unloaded) carrier is slow and rate-limiting at zero membrane voltage and, thus, bestows on the overall reaction cycle a strong voltage dependence over the entire physiological range (*cf.* Fig. 3). Also, the voltage-dependent step, itself, is biased with the ratio $k^o_{78}/k^o_{87} < 1$, so that the carrier must be ''drawn'' across the membrane by depleting state N_8 through substrate binding outside. This characteristic is a necessary consequence of the asymmetry in reaction flow in the cycle *vs.* that of charge movement, and has

the effect of conferring on the carrier cycle a strong interaction between $[NO_3^-]_o$ and membrane voltage (*see* Fig. 10*B*).

(ii) Analogous to the situation for NO_3^- transport in *Arabidopsis*, weightings of the rate constants k_{24} and k_{46} suggest that only one of the two H^+ binding/debinding steps contributes to the steady-state kinetic characteristic for transport in *Neurospora.* Thus the model accommodates a simple Michaelian dependence on $[H^+]_o$, despite the prediction that NO_3^- uptake is stoichiometrically coupled to the influx of *two* H^+.

(iii) As with NO_3^- transport in *Arabidopsis*, the lumped reaction constants κ_{72}, and κ_{27}, that subsume NO_3^- and H^+ binding/debinding inside the cell, are among the fastest steps in the *Neurospora* carrier cycle. The overall effect is to bring the H^+-binding ($N_4 \rightleftharpoons N_2$) and membrane charge-transit ($N_7 \rightleftharpoons N_8$) steps sufficiently close kinetically that they interact (Fig. 10*C*). Such behavior has been described for a number of H^+-coupled or H^+ transporting electroenzymes, including the K^+–H^+ symporter of *Neurospora* (Blatt et al., 1987) and the H^+-ATPases of *Neurospora* [*see* (Hansen et al., 1981)] and *Chara* (Blatt et al., 1990). Although it has been ascribed to a ''proton-conducting well'' structure (Mitchell, 1969), the behavior is readily accommodated within this simple reaction-kinetic scheme [*see also* (Blatt et al., 1987; Hansen et al., 1981; Blatt et al., 1990)]. Note that unlike the *Arabidopsis* transporter, the $N_2 \leftrightarrows N_7$ transition in *Neurospora* is biased toward the unbound state of the carrier (N_7). One expectation is that NO_3^- transport in *Neurospora,* by contrast with the *Arabidopsis* transporter, should be comparatively insensitive to ligand concentrations inside the cell. Nonetheless, since κ_{72} and κ_{27} represent the lumped reaction steps for debinding of NO_3^- and two H^+ a specific prediction is more difficult. We noted that cytoplasmic acid loads reduced the capacity for NO_3^- transport in the induced cells (Fig. 9), so implicating a role for cytoplasmic $[H^+]$ in modulating the activity of the transport system (Ullrich, 1987).

(iv) Finally, the anticipated interactions between chemical substrates outside the cell are at least qualitatively similar, despite the differences in predicted H^+- and NO_3^--binding orders between the two cell types. The NO_3^--binding step in *Neurospora* (k_{86}^o $[NO_3^-]_o$) is kinetically isolated from the rate-limiting H^+-binding transition $N_4 \rightleftharpoons N_2$ by a H^+-binding step that is heavily biased in the forward direction. This transition confers the profound pH_o-dependence to NO_3^- transport at intermediate voltages in *Neurospora* (Fig. 8), like that of the $N_8 \rightleftharpoons N_6$ transition in *Arabidopsis* (Meharg & Blatt, 1995). However, the intervening (''near-irreversible'') H^+-binding step predicts a minimum effect of $[H^+]_o$ on transport and NO_3^- binding at the most negative membrane voltages, as was suggested for *Arabidopsis.* This behavior was actually observed in the present study (*see* Fig. 10*A*).

In conclusion, these analyses highlight the strong dependence of NO_3^- transport in *Neurospora* on membrane voltage as a kinetic parameter and its interaction with extracellular H^+. Our results demonstrate that voltage-dependent restriction of the transport kinetics can account fully for the actions of metabolic blockade with cyanide and of the metabolite NH_4^+. Yet, while it is clear that the voltage parameter is central to the endogenous kinetic regulation of NO_3^- uptake, this level of control speaks only to cells induced for the transport system and not the process of induction itself.

This work was aided by equipment grants from the Royal Society and the University of London Central Research Fund, and was supported by AFRC Research Grant PG32/530 to MRB.

References

Beilby, M., Walker, N.A. 1981. Chloride transport in Chara. I: Kinetics and current-voltage curves for a probable proton symport. *J. Exptl. Bot.* **32:**43–54

Blatt, M.R. 1986. Interpretation of steady-state current-voltage curves: consequences and implications of current subtraction in transport studies. *J. Membrane Biol.* **92:**91–110

Blatt, M.R. 1987*a.* Electrical characteristics of stomatal guard cells: the ionic basis of the membrane potential and the consequence of potassium chloride leakage from microelectrodes. *Planta* **170:**272–287

Blatt, M.R. 1987*b.* Electrical characteristics of stomatal guard cells: the contribution of ATP-dependent, ''electrogenic'' transport revealed by current-voltage and difference-current-voltage analysis. *J. Membrane Biol.* **98:**257–274

Blatt, M.R. 1990. Potassium channel currents in intact stomatal guard cells: rapid enhancement by abscisic acid. *Planta* **180:**445–455

Blatt, M.R. 1991. A Primer in Plant Electrophysiological Methods. *In:* Methods in Plant Biochemistry. K. Hostettmann, editor. pp. 281–321. Academic Press, London

Blatt, M.R. 1992. K^+ channels of stomatal guard cells: characteristics of the inward rectifier and its control by pH. *J. Gen. Physiol.* **99:**615–644

Blatt, M.R., Armstrong, F. 1993. K^+ channels of stomatal guard cells: abscisic acid-evoked control of the outward rectifier mediated by cytoplasmic pH. *Planta* **191:**330–341

Blatt, M.R., Beilby, M.J., Tester, M. 1990. Voltage dependence of the Chara proton pump revealed by current-voltage measurement during rapid metabolic blockade with cyanide. *J. Membrane Biol.* **114:**205–223

Blatt, M.R., Rodriguez-Navarro, A., Slayman, C.L. 1987. Potassium-proton symport in Neurospora: kinetic control by pH and membrane potential. *J. Membrane Biol.* **98:**169–18

Blatt, M.R., Slayman, C.L. 1983. KCl leakage from microelectrodes and its impact on the membrane parameters of a nonexcitable cell. *J. Membrane Biol.* **72:**223–234

Blatt, M.R., Slayman, C.L. 1987. Role of ''active'' potassium transport in the regulation of cytoplasmic pH by nonanimal cells. *Proc. Natl. Acad. Sci. USA* **84:**2737–2741

Breteler, H., Nissen, P. 1982. Effect of exogenous and endogenous

nitrate concentration on nitrate utilization by dwarf bean. *Plant Physiol.* **70:**754–759

Clarkson, D.T., Saker, L.R., Purves, J.V. 1989. Depression of nitrate and ammonium transport in barley plants with diminished sulfate status — evidence of co-regulation of nitrogen and sulfate intake. *J. Exp. Bot.* **40:**953–963

Deane-Drummond, C.E. 1985. Regulation of nitrate uptake in Chara corallina cells via $NH4^+$ stimulation of NO_3-efflux. *Plant Cell Environ.* **8:**105–110

Deane-Drummond, C.E., Glass, A.D.M. 1982. Studies of nitrate influx into barley roots by the use of CL03- 36Cl- as a tracer for nitrate. 1. interactions with chloride and other ions, *Canadian Journal of Botany* **60:**2147–2153

Deane-Drummond, C.E., Glass, A.D.M. 1983*a*. Short term studies of nitrate uptake into barley plants using ion-specific electrodes and 36C103-1: I. Control of net uptake by NO_3-efflux. *Plant Physiol.* **73:**100–104

Deane-Drummond, C.E., Glass, A.D.M. 1983*b*. Short term studies of nitrate uptake into barley plants using ion-specific electrodes and 36C103-1: II. Regulation of NO_3-efflux by NH_{4+} *Plant Physiol.* **73:**105–110

Doddema, H., Hofstra, J.J., Feenstra, W.J. 1978. Uptake of nitrate by mutants of Arabidopsis thaliana disturbed in uptake or reduction of nitrate. I. Effect of nitrogen source during growth on uptake of nitrate and chlorate. *Physiol. Plant* **43:**343–350

Doddema, H., Telkamp, G.P. 1979. Uptake of nitrate by mutants of Arabidopsis thaliana, disturbed in uptake or reduction of nitrate. II. Kinetics. *Physiol. Plant.* **45:**332–338

Eddy, A.A., Hopkins, P.G. 1985. The putative electrogenic nitrate-proton symport of the yeast Candida utilis. *Biophys. J.* **231:**291–297

Felle, H. 1981. Stereospecificity and electrogenicity of amino acid transport in Riccia fluitans. *Planta* **152:**505–512

Glass, A.D.M., Siddiqui, M.Y., Ruth, T.J., Rufty, T.W.J. 1990. Studies of the uptake of nitrate in barley. *Plant Physiol.* **93:**1585–1589

Goldsmith, J., Livoni, J.P., Norberg, C.L., Segel, I.H. 1973. Regulation of nitrate uptake in Penicillium chrysogenum by ammonium ion. *Plant Physiol.* **52:**362–367

Goyal, S.S., Huffaker, R.C. 1986. The uptake of NO3−, NO2−, and NH4+ by intact wheat Triticum aestivum seedlings. I. Induction and kinetics of transport systems. *Plant Physiol.* **82:**1051–1050

Gradmann, D., Hansen, U.-P., Long, W., Slayman, C.L., Warnke, J. 1978. Current-voltage relationships for the plasma membrane and its principle electrogenic pump in Neurospora crassa. I. Steady-state conditions. *J. Membrane Biol.* **29:**333–367

Gradmann, D., Kleiber, H.-G., Hansen, U.-P. 1987. Reaction kinetic parameters for ion transport from steady-state current-voltage curves. *Biophys. J.* **51:**569–585

Hansen, U.-P., Gradmann, D., Sanders, D., and Slayman, C.L. 1981. Interpretation of current-voltage relationships for ''active'' ion transport systems: I. Steady-state reaction-kinetic analysis of class I mechanisms. *J. Membrane Biol.* **63:**165–190.

Hansen, U.-P., Slayman, C.L. 1978. Current-voltage relationships for a clearly electrogenic cotransport system. *In:* Membrane Transport Processes. J.F. Hoffman, Editor. pp. 141–154. Raven Press, New York

Hawkins, H.J., Lewis, O.A.M. 1993. Effect of NaCl salinity, nitrogen form, calcium and potassium concentration on nitrogen uptake and kinetics in Triticum aestivum 1 cv gamtoos. *New Phytologist* **124:**171–177

Heimer, Y.M., Filner, P. 1970. Regulation of the nitrate assimilation pathway in cultured tobacco cells: III. The nitrate uptake system. *Biochim. Biophys. Acta.* **230:**362–372

Henriksen, G.H., Bloom, A.J., Spanswick, R.M. 1990. Measurement of net fluxes of ammonium and nitrate at the surface of barley roots using ion-selective microelectrodes. *Plant Physiol.* **93:**271–280

Henriksen, G.H., Spanswick, R.M. 1993. Investigation of the apparent induction of nitrate uptake in barley Hordeum vulgare L. using NO3–selective microelectrodes. *Plant Physiol.* **103:**885–892

Jackson, W.A., Kwik, K.D., Volk, R.J., Butz, R.G. 1976. Nitrate influx and efflux by intact wheat seedlings: effects of prior nitrate nutrition. *Planta* **132:**149–156

King, B.J., Siddiqi, M.Y., Glass, A.D.M. 1992. Studies of the uptake of nitrate in barley .5. estimation of root cytoplasmic nitrate concentration using nitrate reductase-activity — implications for nitrate influx. *Plant Physiology* **99:**1582–1589

Läuger, P. 1991. Electronic Ion Pumps, Sinauer Press, Sunderland, MA, 1 pp. 1–292

Läuger, P., Stark, G. 1970. Kinetics of carrier-mediated ion transport across lipid bilayer membranes. *Biochim. Biophys. Acta* **211:**458–466

Lee, R.B., Clarkson, D.T. 1986. Nitrogen-13 studies of nitrate fluxes in barley roots. *J. Exptl. Bot.* **37:**1753–1767

Lee, R.B., Drew, M.C. 1989. Rapid, reversible inhibition of nitrate influx in barley by ammonium, *J. Exp. Bot.* **40:**741–752

MacKown, C.T. 1987. Nitrate uptake and assimilation following nitrate deprivation. *J. Exptl. Bot.* **38:**1079–1090

MacKown, C.T., McClure, P.R. 1988. Development of accelerated net nitrate uptake. *Plant Physiology* **87:**162–166

Marquardt, D. 1963. An algorithm for least-squares estimation of nonlinear parameters. *J. Soc. Ind. Appl. Math.* **11:**431–441

McClure, P.R., Kochian, L.V., Spanswick, R.M., Shaff, J.E. 1990. Evidence for cotransport of nitrate and protons in maize roots .1. effects of nitrate on the membrane potential. *Plant Physiology* **93:**281–289

McCulloch, S.R., Beilby, M.J., Walker, N.A. 1990. Transport of potassium in Chara australis: II. Kinetics of a symport with sodium. *J. Membrane Biol.* **115:**129–143

Meharg, A.A., Blatt, M.R. 1995. Nitrate transport in root hairs of Arabidopsis thaliana: kinetic control by membrane voltage and pH. *J. Membrane Biol.* **145:**49–66

Meharg, A.A., Maurousset, L., Blatt, M.R. 1994. Cable correction of membrane currents recorded from root hairs of Arabidopsis thaliana L. *J. Exp. Bot.* **45:**1–6

Miller, A.J., Zhen, R.-G. 1991. Measurement of intracellular nitrate concentrations in Chara using nitrate-selective microelectrodes. *Planta* **184:**47–52

Mitchell, P. 1969. Chemiosmotic coupling and energy transduction, *Theor. Exptl. Biophys.* **2:**159–216

Privalle, L.S., Lahners, K.N., Mullins, M.A., Rothstein, S. 1989. Nitrate effects on nitrate reductase activity and nitrite reductase mRNA levels in maize suspension cultures. *Plant Physiol.* **90:**962–967

Rao, K.P., Rains, D.W. 1976. Nitrate absorption by barley. I. Kinetics and energetics. *Plant Physiol.* **57:**55–58

Redinbaugh, M.G., Campbell, W.H. 1991. Higher plant response to environmental stress. *Physiol. Plant* **82:**640–650

Rodriguez-Navarro, A., Blatt, M.R., Slayman, C.L. 1986. A potassium-proton symport in Neurospora crassa. *J. Gen. Physiol.* **87:**649–674

Rufty, T.W., Jr., MacKown, C.T., Israel, D.W. 1990. Phosphorus stress effects on assimilation of nitrate. *Plant Physiol.* **94:**328–333

Sanders, D., Hansen, U.-P. 1981. Mechanism of Cl^- transport at the plasma membrane of Chara corallina: II. Transinhibition and determination of H^+/Cl^- binding order from a reaction kinetic model. *J. Membrane Biol.* **58:**139–153

Sanders, D., Hansen, U.-P., Gradmann, D., Slayman, C.L. 1984. Gen-

eralized kinetic analysis of ion-driven cotransport systems: a unified interpretation of selective ionic effects on Michaelis parameters. *J. Membrane Biol.* **77:**123–152

Sanders, D., Slayman, C.L. 1982. Control of intracellular pH: predominant role of oxidative metabolism, not proton transport, in the eukaryotic microorganism Neurospora. *J. Gen. Physiol.* **80:**377–402

Sanders, D., Slayman, C.L., Pall, M. 1983. Stoichiometry of H^+/amino-acid cotransport in Neurospora crassa revealed by current-voltage analysis. *Biochim. Biophys. Acta* **735:**67–76

Schloemer, R.H., Garrett, R.H. 1974. Nitrate transport system in Neurospora crassa. *J. Bacteriol.* **118:**259–269

Schwab, W., Komor, E. 1978. A possible mechanistic role of the membrane potential in proton-sugar cotransport of Chlorella. *FEBS Lett.* **87:**157–160

Segel, I.H. 1993. Enzyme Kinetics, Wiley Interscience, New York

Slayman, C.L. 1977. Energetics and control of transport in *Neurospora. In:* A.M. Jungreis, T.K. Hodges, A. Kleinzeller and S.G. Schultz, editors. Water Relations in Membrane Transport in Plants and Animals. pp. 69–86. Academic Press, New York

Slayman, C.L., Bertl, A., Blatt, M.R. 1994. Partial reaction chemistry and charge displacement by the fungal plasma-membrane H^+-ATPase. *In:* Molecular and Cellular Mechanisms of H^+ Transport. :B.H. Hirst, editor. pp. 237–244. Springer Verlag, Berlin

Slayman, C.L., Gradmann, D. 1975. Electrogenic proton transport in the plasma membrane of *Neurospora. J. Gen. Physiol.* **15:**968–971

Slayman, C.L., Slayman, C.W. 1974. Depolarization of the plasma membrane of Neurospora during active transport of glucose: evidence for a proton-dependent cotransport system. *Proc. Natl. Acad. Sci. USA* **71:**1935–1939

Slayman, C.W., Tatum, E.L. 1968. Potassium transport in *Neurospora.* I. Intracellular sodium and potassium concentrations, and cation requirements for growth. *Biochim. Biophys. Acta* **88:**578–592

Smith, F.A. 1973. The internal control of nitrate uptake into excised barley roots with differing salt contents. *New Phytol.* **72:**769–782

Tischner, R., Waldeck, B., Goyal, S.S., Rains, W.D. 1993. Effect of nitrate pulses on the nitrate-uptake rate, synthesis of mRNA coding for nitrate reductase, and nitrate-reductase activity in roots of barley seedlings. *Planta* **189:**533–537

Ullrich, W.R. 1987. Nitrate and ammonium uptake in green algae and higher plants: mechanism and relationship with nitrate metabolism. *In:* W.R. Ullrich, . pp. 32–41. Inorganic Nitrogen Metabolism, Springer Verlag, Berlin

Ullrich, W.R., Larsson, M., Larsson, C.M., Lesch, S., Novacky, A. 1984. Ammonium uptake in Lemna gibba g-1, related membrane potential changes, and inhibition of anion uptake, *Physiologia Plantarum* **61:**369–376

Ullrich, W.R., Novacky, A.J. 1981. Nitrate-dependent membrane potential changes and their induction in Lemna gibba G1, *Plant Sci. Lett.* **22:**211–217

Ullrich, C.I., Novacky, A.J. 1990. Extracellular and intracellular pH and membrane-potential changes induced by K^+, Cl^-, $H_2PO_4^-$, and NO_3- uptake and fusicoccin in root hairs of Limnobium stoloniferum. *Plant Physiol.*. **94:**1561–1567

Vogel, H.J. 1956. A convenient growth medium for *Neurospora* medium N. *Microb. Genetics* **13:**42–46

Wegmann, D., Weiss, H., Ammann, D., Morf, W.E., Pretsch, E., Sugahara, K., Simon, W. 1984. Anion-selective liquid membrane electrodes based on lipophilic quaternary ammonium compounds. *Mikrochim. Acta* **3:**1–16

Zhen, R.-G., Koyro, H.-W., Leigh, R.A., Tomos, A.D., Miller, A.J. 1991. Compartmental nitrate concentrations in barley root cells measured with nitrate-selective microelectrodes and by single-cell sap sampling. *Planta* **185:**356–361